RM-312

POLARIMETRIC MEASUREMENTS OF SIMULATED LUNAR SURFACES (PHASE II)

February 1966

Grumman

RESEARCH DEPARTMENT

GRUMMAN AIRCRAFT ENGINEERING CORPORATION

BETHPAGE NEW YORK

Grumman Research Department Memorandum RM- 312

POLARIMETRIC MEASUREMENTS OF SIMULATED LUNAR SURFACES

(PHASE II)

by

W. G. Egan

and

L. L. Smith

Geo-Astrophysics Section

February 1966

Second Interim Report on Contract NAS 9-4942

Approved by: Charles E. Mack, Jr.

Charles E. Mack, Jr.
Director of Research

ACKNOWLEDGEMENTS

The authors wish to acknowledge the exceptional efforts of H. B. Hallock, J. Grusauskas, D. R. Lamberty, and D. Schlaijker in perfecting the polarimetric analyzer and for recording and reducing data. We wish to give thanks also to C. Bartallata, C. Germann, C. Krolik and D. Yustein for their assistance.

We are also grateful to the following individuals for discussions in relation to the pursuit of the program: J. Halajian, H. Hallock, Dr. G. McCoyd, Dr. N. Milford, J. Reichman, Dr. M. Sidran and F. Spagnolo.

TABLE OF CONTENTS

LIST OF ILLUSTRATIONS

INTRODUCTION AND SUMMARY

This is the second of three interim reports on "Polarimetric Measurements of Simulated Lunar Surfaces," an investigation conducted under Contract No. NAS 9-4942. This report covers work accomplished with pulverized specimens during Phase II under the provisions of Proposal B.

As a result of Phase I conducted under this contract (Ref. 1), it was found that Volcanic Ashes Nos. 1 and 4 and Coral No. 1 possessed average properties that could vary sufficiently in detail to permit them to be considered as polarimetric models of the lunar surface. Two other materials (Furnace Slag No. 1 and Copper Oxide) could be considered as having appropriate properties when combined with a suitable nonpolarizing material with the albedo varying as a function of phase angle.

The present investigation was undertaken to lay the basis for an analytical approach. Thus, the polarization properties of materials were investigated as a function of particle size, albedo and porosity, since current theories of polarization indicate some of these properties as significant parameters.

In the conclusions of Phase I, it was mentioned that previously reported models such as those of Lyot, Dollfus, Gehrels, Hapke and Wehner are not unique. This was borne out by the recent LUNA-9 photographs (Ref. 2). However, it appears that there is a commonality that exists among models such that we may use all the data on hand (photometric, thermal, and mechanical) to evaluate appropriate polarimetric models that conform to the requirements.

Apparently, to obtain the proper polarimetric signature, consistent with a good photometric signature, (Refs. 3 and 4) the coarse structure (which can only be observed on a large scale photometer such as the Grumman unit) producing proper shadowing for photometry must be modified in some way. This modification could occur from an overcoat of powder or possibly a surface modification by proton bombardment. If the modification is by a powder coating, it appears from the present work that certain particle size ranges produce the proper signature based on a least squares curve fit of per cent polarization. The laboratory data has been analyzed in terms of lunar maria (Crisium) and highland (Clavius) curves. The best fit to Mare Crisium

is obtained with Furnace Slag No. 4 particles less than 37 microns (Fig. 15), Volcanic Ash No. 4 between 37 and 88 microns (Fig. 8), Volcanic Ash No. 1 greater than 0.21 mm (Fig. 23), the sponge-like slag obtained at NASA (Fig. 27), and the Ash from Vesuvius (Fig. 25). For Clavius, Furnace Slag No. 1 less than 1 micron (Fig. 15), Volcanic Ash No. 4 between 1 and 37 microns (Fig. 8), and Volcanic Ash No. 1 less than 1 micron (Fig. 23) are best fits.

This surface coating is not ruled out by the resolution of 2 mm given by the LUNA-9 photographs (Ref. 5). A powder thin enough to be consistent with the LUNA-9 pictures would not affect the bearing strength of the underlying "rock". It appears possible to draw certain inferences about the limits to be placed on the thermal inertia constant, γ, based on a two layer model of the lunar surface. A two layer thermal model of the lunar surface has been analyzed (Ref. 6), and it is applied to a high γ (porous) upper layer and a low γ under layer. The particle size limits in such a layer can be inferred from the present work, to be between 1 micron and somewhat over 0.21 mm depending upon material.

The sponge-like slag obtained at NASA/MSC appeared to yield the improper inversion angle and minimum.

TEST EQUIPMENT

Description

The test equipment described in the Phase I report (Ref. 1) has been improved under a Grumman-supported program. During the calibration and measurements of Phase I, there appeared to be a residual non-uniform 1% polarization in the collimated light beam illuminating the sample. There also appeared to be an additional 1% residual polarization in the 60 degree polarimeter above the zero degree polarimeter. In addition, there was an apparent rotation of the observed plane of polarization with phase angle.

As a result of extensive observations, measurements, and analyses of the equipment, these effects have been appreciably reduced, eliminated or clarified.

Source Polarization – The collimated light from the source was analyzed on the sample table with a test jig using a 6199 end window photomultiplier. Initially, the jig utilized a plastic polaroid, but this was replaced by a glass sandwich HN-22 polaroid for higher precision. It was then found that there was an overall positive asymmetric polarization bias from the source. By a process of elimination, it was found that the largest contributor to the polarization was the tungsten-iodine 1000 watt lamp itself. Two ground quartz diffuser discs in front of the lamp were found to be inadequate to remove the residual polarization. But by following the two diffuser discs with an opal glass, the polarization was reduced to a small value. The source lens was found to be non-contributory to the average residual polarization following checks with a frosted incandescent lamp. The rhodium mirrors were realigned following replacement of one which had some pin holes in it. The field stop in the source was opened up to smear out the nonuniformities in the field and allow more light through. This also increased the beam divergence from 1/2 degree to 2 degrees. The result was a nearly symmetrical beam with a residual polarization of about 1% at the center. However, the planes of the residual polarization of the source were not exactly parallel or perpendicular to the plane of vision at the four cardinal points as they should be if the source were perfect; they were found at varying intermediate angles.

At present, we expect to further improve the situation by replacing the other rhodium mirror which has some pin holes, realigning the source field stop, and replacing the tungsten-iodine lamp with a frosted one. This will be done prior to Phase III.

Photometer-Polarimeter Polarization – The zero degree polarimeter was checked for residual polarization by placing a frosted lamp behind a ground glass and located where the photomultiplier would be. The collimated light from this arrangement was examined on the sample table with the test jig. The residual polarization was found to be of the order of +1/4 of a percent due mainly to the residual polarization of the source used. An alternate method was used to recheck the overall polarization of both polarimeters following the measurements. This consisted of using a frosted incandescent lamp under a 2-inch square plate of opal glass covered by a mylar diffusing screen as the source being observed by the polarimeters. The polarization of this configuration was measured on the polarimeter by rotating the polaroid; then the source was rotated 90 degrees about the viewing direction and the polarization remeasured. This rotation of the source was done to check that no residual polarization existed in the source.

However, in Phase I, the sixty degree polarimeter was observed to have a residual polarization of about 1% above that of the zero degree polarimeter. After other variables had been eliminated, the 7 element, 12 inch f/2.5 Aero Ektar field lens was found to have a small separation at the center of one of the three cemented elements. This lens was replaced with another, and the residual polarization was then found to be about 1/4 percent.

Rotation of Plane of Polarization – Calibration curves were run with a 1 inch thick glass plate held in the incident beam by another jig. This jig served to locate the front surface of the glass plate exactly on the axis of rotation of the source. It was found that the source was still not sufficiently depolarized to permit the application of Fresnel's equations to the glass plate to check per cent and plane of polarization. Hence, an additional depolarizer was inserted into the same beam below the mirrors. This depolarizer consisted of another opal glass and a frosted mylar diffuser. Agreement was then obtained for the position of the plane of polarization within a fraction of a degree when a simultaneous calibration was made to monitor the gain of the potentiometer recorder used in the measurements.

Calibration

Per Cent Polarization — The per cent polarization calibration of the overall system is twofold: first, the residual polarization of the source assembly (the lamp, diffusers, lens, and two rhodium front surface mirrors) is checked at the position of the sample table with the 6199 photomultiplier test jig; second, the residual polarization of the two polarimeters is checked by the techniques mentioned under "Description" and by reflection from a one inch thick glass plate using the source beam.

The residual polarization of the source must be checked over the entire 3 inch diameter field viewed by the polarimeters at the same voltage applied to the lamp for observations. During the measurements of Phase II, a lamp voltage lower than the rated was used to prevent the photomultipliers from saturating. The higher available lamp intensity at rated voltage is necessary for Phase III for measurements in the I (0.94μ) region, where the filter assembly cuts the light down considerably. The lower lamp voltage as well as the combination of two diffusers and an opal glass redden the source somewhat. The system color response was determined by the use of narrow band interference filters and was found to be centered at a wavelength of $0.52 \pm 0.01\mu$ for the lamp voltage used. When albedos were measured, a still lower voltage was used for comparison to the magnesium carbonate block for the same reason. The color response of the system at this lower voltage was measured and found to be centered at $0.56 \pm 0.01\mu$.

The polarimeter jig with the 6199 photomultiplier was checked for residual polarization with an unpolarized light source (frosted bulb plus diffusers) and found to have about a tenth of a per cent.

The polarimeters were checked, as in Phase I, by applying Fresnel's equations to a glass plate (index 1.52) at small phase angles, and calculating the per cent polarization. The glass plate was then carefully positioned for specular reflection from the source (see above) into either the zero or 60 degree polarimeter, and a measurement of per cent polarization made. Agreement within experimental error of a few tenths of a per cent was expected and obtained. The upper glass plate surface was positioned exactly at the center of rotation of the source. The 6199 photomultipliers were operated at 820 volts for Phase II.

Plane of Polarization – The plane of polarization is initially determined using the glass plate as in the "Per Cent Polarization" calibration. From Fresnel's equations, the plane of polarization from the glass plate is perpendicular to the plane of vision. Thus, this position can be used as an absolute reference for the polaroid used to observe the plane of polarization of the samples observed. Hence, a sine curve may be run for a complete rotation of the polaroid analyzer in the zero or 60 degree polarimeters while observing the glass plate at a phase angle at something greater than zero degrees. The relative displacement of the sine curve obtained by a rotation of the polaroid analyzer, while observing the glass plate with the polarimeter, gives the absolute position of the plane of polarization relative to the plane of vision (see Ref. 1, Appendix).

The glass plate must be set up at the position of the sample (with the sample table removed), and accurately located and positioned for specular reflection. Then the sample table is replaced with the sample, and the position of the plane of polarization measured for various phase angles. Because of the time consuming nature of this process, a simplified technique was devised using a fixture that holds an HN-22 polaroid at an angle of 60 degrees from the horizontal in a precisely fixed position on the sample table. This fixture is used as a secondary standard to locate the reference for the plane of polarization conveniently. The position of the HN-22 polaroid is positioned to a fraction of a degree parallel to that given by the glass plate for both polarimeters. The accuracy of the polaroid reference is augmented by increasing the recording amplifier gain during the measurement, and subtracting the increased DC reference level with a bucking out circuit.

Standard Polarimetric Curves and Data Presentation

Although the best data in integrated lunar light seem to be that of Lyot (Ref. 7), it appears that, as lunar and laboratory data become more refined, a range of values should be considered to differentiate the lunar maria from the highlands. The best detailed regional lunar polarization data appears to be that of Gehrels, Coffeen and Owings (Ref. 8). The Russian observations appear to be inaccurate because of a large residual polarization in the instrumentation (see Ref. 9). Since Gehrels, et. al., made spectral observations, a comparison will be made of the integrated visual data of this report and their $G(0.54\mu)$ data

as the closest approximation. The two areas that had the most complete lunation curve, including the maximum, with the greatest extremes in polarization were Mare Crisium and Clavius. Other curves depicted slightly higher maximum polarization, but because of problems in the observation of certain lunar phase angles, the curves were incomplete. Crisium and Clavius are representative of lunar maria and highlands (a crater floor) with corresponding low and high albedos, and high and low polarization respectively. The curves are shown in Fig. 1, together with the curve of Lyot formerly used (Ref. 1). The maxima are seen to be 12.5 and 5.8 per cent compared to 7.7 per cent of Lyot. The minimum of Clavius is -0.9 and that of Crisium and Lyot is -1.2 per cent. The inversion angles also differ: Mare Crisium, 23.7°, Lyot (average) 23.5°, and Clavius, 25.0°. The phase angle at maxima of Lyot (average) and Crisium are the same (102°), but the brighter Clavius has the maximum at 91°.

By refining the data analysis on the basis of these curves, it may be possible to determine, from polarization observations, the characteristics of a typical maria and highland surface.

It should be pointed out that the curves for Mare Crisium and Clavius are averages of observations for positive and negative phase angles in Gehrels et al. (Ref. 8).

As mentioned in Gehrels' paper, the polarization observed in 1963 was higher, presumably due to lunar luminescence. This is also inferred from their visual brightness measurements showing brighter areas in 1956 or 1959 (when the sun was active in producing a high level of ionizating radiation), compared to 1963 and 1964. Hence, the albedos used in this report are averages of the two values obtained at those times.

According to Gehrels (Ref. 8) the existence of lunar luminescence could be inferred from not only the albedo data but from the polarization data, where the polarization is lower in 1956 and 1959 indicating a non-polarizing (luminescence) component in the polarization observation.

To explain the reduced polarization, it is not necessary to require the luminescent light to be unpolarized. In fact, as long as the per cent polarization of the luminescent light is smaller than the per cent polarization of the non-luminescent light, the addition of luminescence will reduce the observed polarization percentage. This will be elaborated upon in Phase IV.

PHASE II – PULVERIZED SPECIMENS

Purpose

Phase II has the objective of laying the basis for an analytical approach to the polarization properties of materials. Since current theories of polarization indicate that particle size, albedo and porosity are significant parameters, these will be investigated. Materials will be those of Phase I, whether or not they proved satisfactory polarization models, plus some additional ones.

Test Specimens

The light scattered from the contractually required specimens was analyzed polarimetrically for the per cent polarization and position of the plane of polarization. The following pulverized specimens were investigated:

Volcanic Ash No. 4 and Furnace Slag No. 4 in the following sizes:

a) 2.83 mm to 6.35 mm

b) 1.19 mm to 2.83 mm

c) 0.50 mm to 1.19 mm

d) 0.21 mm to 0.50 mm

e) 0.088 mm to 0.21 mm

f) 0.037 mm to 0.088 mm

g) $\leq$ 0.037 mm

h) $\leq 1\mu$

(It is to be noted that Furnace Slag No. 4 was substituted for Furnace Slag No. 1 in order that the sample not be destroyed as mentioned under Phase I.)

Coral, Silver Chloride, Copper Oxide and Volcanic Ash No. 1 in the following sizes:

a) 0.088 mm to 0.21 mm

b) $\leq$ 1μ

The properties of per cent polarization and position of the plane of polarization are determined as a function of phase angle and simulated lunar longitude in integrated visual light ($0.52 \pm 0.01\mu$).

In addition, Vesuvius Ash, and two furnace slags furnished by NASA/MSC were checked for polarization, and a sample of Lyot's volcanic ash was examined microscopically.

Sample Preparation

The larger size particles were obtained by coarse pulverization in a rock crusher and sieving. The finer particles (below about 0.21 mm), other than silver chloride and coral, were obtained by stainless steel ball milling the larger particles and sieving. The smallest particles were obtained by subjecting the particles below 0.037 mm to processing by a Helme Fluid Energy Mill (Fig. 2). The Fluid Energy Mill is a device that converts a compressed gas into an energy exchange mechanism that causes the particles of a material to be thrown together with such velocities as to cause them to break up into micron and submicron particles. The fineness of the grind depends upon the gas pressure used, the nozzle adjustments, and the number of times the particles are fed through the machine. Dry nitrogen was used as the grinding medium.

The coral was reduced in size in a porcelain mortar and pestle (so as not to contaminate the surface with metallic particles from a ball mill), and subsequently ground in the fluid energy mill.

The larger sizes of silver chloride were obtained as a powder. The smallest size was obtained as a precipitate of silver chloride from a silver nitrate solution using hydrochloric acid, and dried in a thin layer. An alternative larger powder sample was ground up to a 2 to 3 micron size in the fluid energy mill, before it clogged the mill. Silver chloride is ductile and is not readily ground. The particles obtained from the mill were examined in a dispersed form under a microscope for proper required sizes (see Fig. 3).

This Figure (3) shows that there is still evidence of non-dispersed agglomerates of particles (visible in Fig. 3a). Figures 3a, b, c, d, f, and h are "bright field" illumination, wherein the collimated light from the source impinges directly upon the upper surface of the specimen, and the specimen is viewed in reflected light. Figures 3e and g are "dark field," wherein they are illuminated obliquely, resulting in their being visible by refracted and obliquely reflected light. The advantage of the dark field illumination is that one may gain some insight into the transparency and refraction properties of a substance by microscope observation. There was no problem with obtaining particles 1 micron or less of the Volcanic Ashes, Furnace Slag, Coral or Copper Oxide (Figs. 3a, b, c, d, and h). The silver chloride precipitate agglomerates, but the individual particles are well below a micron in size (Fig. 3e). The silver chloride that resulted from the fluid energy mill grind (sizes from 3 to 8 microns) is shown in Figs. 3f and g under bright and dark field illumination. Agglomeration is evident. Because of the non-dispersed effect of the silver chloride precipitate layer, the 3-8 micron silver chloride powder was also examined for polarization as an extra sample.

Samples were carefully dispersed over the sample area on the polarimeter, covering the backing board completely in the viewing area.

The finest particles tended to agglomerate because of the high strength of the surface forces.

Some additional specimens, not required by the contract, were examined. These were:

(a) Ashes from the side of the cone of Vesuvius, obtained by one of the authors (W.G. Egan) June 1, 1965.

(b) Two furnace slag samples, obtained by one of the authors (W.G. Egan) at the NASA/MSC astronaut simulation pit on March 16, 1965; one was sponge-like and the other appeared rusty, suggesting iron.

(c) Ashes of Vesuvius, April 14, 1908, used in the Lyot Configuration, (Ref. 7, 109 - Thesis p. 120), Curve E, Albedo 0.166; this sample was kindly furnished to one of the authors (W.G. Egan) by Prof. A. Dollfus, May 1965.

Experiments

Percent Polarization

The percent polarization as a function of phase angle for the six required and 4 additional samples is presented graphically in Figs. 5 through 27 and Table 1.

The data can be analyzed conveniently for the contractually required specimens in five sections:

1. Effect of Albedo
2. Effect of Particle Size
3. Effect of Porosity
4. Effect of Material
5. Effect of Simulated Lunar Longitude

The remaining samples (Vesuvius Ash, two Furnace Slags furnished by NASA/MSC and Lyot Volcanic Ash) are examined in percent polarization and albedo for the first three and microscopically for the last.

Thus, the percent polarization data are presented for each of the observed samples in terms of comparison graphs, along with the curves for Mare Crisium and Clavius.

Plane of Polarization

The plane of polarization for the above six required samples was analyzed as a function of phase angle, referenced to the secondary polaroid standard, which was aligned to the plane of vision determined by the glass plate. The data are presented in Table 2.

Discussion of Test Results

Effect of Albedo

A relationship between albedo and polarization has been observed for the lunar surface (see, for instance, Lyot Ref. 7); the lower the albedo, the higher the maximum observed polarization. This may be conveniently seen for the laboratory observations by reference to Table 1, which is essentially a summary of the graphical information contained within Figs. 5 through 27, but which has

Table 1

DATA ANALYSIS

PERCENT POLARIZATION

Furnace Slag No. 4

Size Range	Average Albedo	Percent Porosity	Maximum %	Maximum Angle	Minimum %**	Minimum Angle	Inversion** Angle	Apparent Density g/cm^3	Real Density g/cm^3
a) 2.83 to 6.35 mm	.085	65*	41	117°	-0.8	10°	18.5°	1.59*	4.4*
b) 1.19 to 2.83 mm	.080	56*	40	116	-0.9	9	17.5	1.97*	4.8*
c) 0.50 to 1.19 mm	.075	60*	46	117	-1.0	8?	17.0	1.82*	4.9*
d) 0.21 to 0.50 mm	.070	58*	47	122	-1.0	9?	18.5	1.90*	4.6
e) 0.088 to 0.21 mm	.070	60*	46	123	-0.9	9	17.0	1.78*	4.3*
f) 0.037 to 0.088 mm	.095	65*	20	109	-0.9	9	17.5	1.60*	4.5*
g) ≤ 0.037 mm	.105	68*	14	111	-0.7	9	18.5	1.44*	4.3*
h) ≤ 1μ mm	.140	76	9	115	-0.8	11?	23.0	1.00	4.2
Volcanic Ash No. 1									
0.088 to 0.21 mm	.150	67	8.4	93.5	-1.4	10	24.5	1.10	3.3
≤ 1μ	.175	80	5.8	99.0	-1.2	10	25.0	0.50	2.5
Volcanic Ash No. 4									
a) 2.83 to 6.35 mm	.135	71*	16.6	104	-1.4	2.5?	21.0	0.85*	2.72*
b) 1.19 to 2.83 mm	.125	64*	17.6	106	-1.3	6?	21.5	1.00*	2.94*
c) 0.50 to 1.19 mm	.120	60*	18.1	106	-1.4	6?	23.0	1.16*	3.05*
d) 0.21 to 0.50 mm	.125	53*	17.5	113	-1.7	10	23.5	1.38*	3.05*
e) 0.088 to 0.21 mm	.125	55*	16.0	109	-1.5	11	22.5	1.31*	3.00*
f) 0.037 to 0.088 mm	.130	59*	13.4	107	-1.3	11?	22.5	1.20*	2.82*
g) ≤ 0.037 mm	.165	73*	6.7	92	-1.2	9	20.5	0.80*	2.93*
h) ≤ 1μ	.195	75	4.8	105?	-1.0	12	24.0	0.70	2.80
Coral No. 1									
0.088 to 0.21 mm	.54	53	>2.4	>125°	<-0.5	4.5°	29.0°	1.24	2.7
≤ 1μ	.71	81	>1.4	>125	<-0.4	7	27.5	0.53	2.8
Copper Oxide									
0.088 to 0.21 mm	.04	72	75.5	125	-0.8	7	17.5	1.74	6.2
≤ 1μ	.06	73	66	121	-0.7	7.5	14.5	1.71	6.2
Silver Chloride									
0.088 to 0.21 mm	.09	63	>69	>125	-0.9	5	15.0	2.22	6.0
3 to 8μ	.09	67	>35	>125	-0.8	5	17.0	1.85	5.6
≤ 1μ	.12	-	48	120	-0.9	12	26.5	-	-
Miscellaneous Samples									
Vesuvius Cinders	.13	-	>15	>118	-1.2	10	22.5	-	-
Slag (Sponge-like)	.11	-	>24	>125	-0.8	3	15	-	-
Slag (with rust)	.08	-	>47	>125	-0.9	6	15	-	-
Lunar Comparison									
Clavius	.268	-	5.8	91	-0.9	11	25.0	-	-
Crisium	.137	-	12.5	102	-1.2	11	23.7	-	-
Lyot (average)	.11	-	7.7	102	-1.2	11	23.5	-	-

* From Ref. 3.

** Corrected for + 1/4% instrumental error.

been corrected for the residual polarization of +0.25% found in the 0° and 60° polarimeters. The albedos measured are to an accuracy of ±0.01, which is consistent with the values given in Halajian (Ref. 3).

Consider, for example Furnace Slag No. 4 (curves in Figs. 12 through 15). For the smallest particle sizes, the albedo is highest, and the maximum polarization the smallest. Through an intermediate range of particle sizes up from 0.21 mm to 0.50 mm, the polarization increases as the albedo decreases; then, going to larger particles, the polarization decreases as the albedo increases.

It appears that as the particles are made finer, they become transparent. This was verified by microscope observations (see Fig. 3). It is then expected that the refracted component of the incident light (negative polarization) becomes stronger relative to the reflected component (positive polarization). Thus, as observed, one would expect the negative component to counterbalance a larger part of the positive component and reduce the maximum positive polarization observed for the intermediate size particles.

However, for the largest particles of furnace slag, an anomalous effect occurs. Because of a white surface coating on some of the slag particles (not extending to the interior), the albedo increases for larger particle sizes. This increased albedo could lower the polarization by multiple reflection effects, but can be misleading as to porosity inferences (see following discussions on Particle Sizes and Porosity).

The Volcanic Ash No. 4 (Figs. 5 through 8) shows the same tendency for maximum polarization as a function of particle size for the smaller particles. However, on both the Volcanic Ash No. 4 and Furnace Slag No. 4 (and also the moon - see Table 1) as the albedo decreases, the maximum moves to larger phase angles, contrary to the theoretical analysis of Hapke (Ref. 10), who assumes a nonpolarizing component given by the Schoenberg reflection formula for a diffusely-reflecting sphere.

Copper oxide, Fig. 21, with the lower albedo as compared to the silver chloride (Fig. 20), does not clearly have the higher polarization. This is probably due to metallic silver particles formed when the silver chloride was exposed to light, possibly causing a large scattered positive polarization component.

Coral (Fig. 19), being quite translucent in the smaller particles, has a low positive polarization. The coral is presumed to be mainly calcium carbonate.

Volcanic Ash No. 1, (Fig. 23) having a lighter brownish color, has a lower polarization because of the higher albedo.

In an over-all comparison, there appears to be no clear relationship between the inversion point or the minimum polarization and albedo on these samples.

Effect of Particle Size

There appears to be a relationship between albedo and particle size; this was pointed out by Halajian (Ref. 3) for Furnace Slag No. 4 and Volcanic Ash No. 4. Our work indicates this to be true for small particle sizes, but an extraneous effect appears for larger particle sizes. Because of a white coating on some of the largest furnace slag specimens, the albedos of the large particles measured higher than would be expected if the particles were homogeneous between the surfaces and the interior.

Thus, the relationship of higher albedo for smaller particle sizes holds only below about 0.50 mm particles.

The inversion angle appears to be greatest for medium size particles (excluding the below 1 micron particles) of Volcanic Ash No. 4. The negative minimum shows a similar effect in both volcanic and No. 4 and Furnace Slag No. 4.

Effect of Porosity

Referring to Table 1, it is seen that the porosity and albedo appear to follow the same trend for the smaller particles below about 0.50 mm in size for Volcanic Ash No. 4 and Furnace Slag No. 4. For the larger sizes, there is the previously mentioned misleading surface effect that causes an increase in albedo for Furnace Slag No. 4.

Thus, the trend of increasing porosity (and decreasing apparent density, see Ref. 3) with increasing albedo only occurs for particles below about 0.50 mm. The real densities do not vary appreciably.

Effect of Material

The primary effect of the material is in respect to the complex index of refraction. For transparent or translucent materials (low

imaginary component of the complex index of refraction) the magnitude of the positive maximum is decreased. The real component along with the complex portion, the particle size, and the particle shape possibly influences the inversion and the negative minimum.

Longitude Independence

Referring to Figs. 9 and 10 (Volcanic Ash No. 4), Figs. 16 and 17 (Furnace Slag No. 4), and Volcanic Ash No. 1 (Fig. 23), there appears to be a slightly higher average positive percent polarization on the 60 degree polarimeter.

Within the experimental errors, no longitude dependence is discerned for coral (Fig. 19), silver chloride (Fig. 20), or copper oxide (Fig. 21).

Miscellaneous Samples

Vesuvius cinders - these samples (Fig. 24) of cinders (about 3 mm average diameter) were picked up by one of the authors (W.G. Egan) within about 1000 feet of the top of the volcano. Of course they have been subject to weathering and erosion, but they were thought to offer some promise in lunar simulation based on the work of Lyot on smaller samples (see Fig. 28a, b). The Lyot sample (furnished by Prof. A. Dollfus) was one of the two sizes of Vesuvius Ash that were combined to reproduce the average lunar polarization curve. There are particles of approximately 210 microns (Fig. 28b) as well as those of a few microns in size (Fig. 28a). This assortment would be expected to give a resulting polarization made up of a "weighted" average of the particles in that range. The smallest particles are somewhat translucent.

It is interesting to compare the bright and dark field photographs of copper oxide powder (Figs. 28c, d). In bright field illumination (Fig. 28c) the copper oxide is opaque, but in dark field (Fig. 28d), the copper oxide looks like speckled glass with many reflecting or diffracting facets.

However, small particles of coral (Fig. 28e) look like rock candy under the microscope.

Volcanic Ash No. 1 (Fig. 28f) appears as an assortment of light and dark brown transparent grains.

The observed polarization on the Vesuvius Cinders is depicted in Fig. 25.

Furnace slags - these samples (Fig. 26) of blast furnace slag were picked up by one of the authors (W.G. Egan) during a visit to NASA/MSC on March 16, 1965. They were obtained from the pit used for astronaut lunar simulation. One sample was dark, sponge-like in appearance, and light in weight. The other sample was also dark but denser, and appeared to be dispersed with iron, giving it a rusty appearance. The observed polarizations are shown in Fig. 27.

Plane of Polarization

The observations made on the position of the plane of polarization are listed in Table 2, referenced to the secondary polaroid standard, which has been aligned to the plane of vision as determined by the glass plate reference. Polaroid alignment to the glass plate was made at 128° and 68° phase angles on the 60° and 0° polarimeters. The accuracy of alignment was checked through the range of smaller phase angles for both polarimeters, and alignment was to within a fraction of a degree.

In the observations listed in Table 2, the angular displacement of the plane of polarization follows the convention in the Appendix of Ref. 1. Angles greater than 90 degrees are considered negative to make the data easily readable (i.e., $\theta_r = -95°$ is identical to $\theta_r = +85°$).

Referring to Table 2, we may draw the following conclusions:

1. There is general agreement between the inversion angle determined from the corrected percent polarization data and the plane of polarization data;

2. The angular shift in the plane of polarization from 0° to 90° at inversion is more rapid with the 60° polarimeter as compared to the 0° polarimeter;

3. There is a general negative drift in the 0° position of the plane of polarization as observed with the 0° polarimeter with decreasing phase angle; the 60° polarimeter does not show this. Hence, a possible instrumental effect is suggested as an explanation.

Table 2

PLANE OF POLARIZATION OBSERVATIONS

FURNACE SLAG NO. 4

Particle Size	Zero Degree Polarimeter				60 Degree Polarimeter			
	Date	Inversion Angle	Phase Angle	θ_r	Date	Inversion Angle	Phase Angle	θ_r
2.83 to 6.35 mm	2/4/66		68°	-2°	2/4/66		128°	0°
		18.5°	21	-8.5			59	-1
			15	-78.5		18.5°	24	-8
			11	-83			10	-91.5
			9	-84			7	-94
1.19 to 2.83 mm	2/4/66		68	+2.5	2/4/66		128	-1
			36.5	+1			62.5	-1
			28	-1.5			32.5	-1.5
		17.5	21	-13.5		17.5	24	-2
			14	-83.5			14	-93
			7.5	-80.5			7	-92
0.50 to 1.19 mm	2/5/66		68	-1.5	2/5/66		128	-1
			29.5	-2.5			63	-0.5
			21	-7.5		17.0	20	-3.5
		17.0	19	-20			11.5	-88
			15	-85.5			6	-90
			11	-84.5				
0.21 to 0.50 mm	2/5/66		68	-0.5	2/5/66		128	0
			24	+0.5			57	0
		18.5	20	-4			28	+0.5
			15.5	-65		18.5	21	+0.5
			6	-77.5			12	-97.5
							7.5	-89.5
0.088 to 0.21 mm	2/5/66		68	0	2/5/66		128	0
			23	-1			58.5	-0.5
		17.0	19.5	-4			21.5	-6
			14	-63.5		17.0	20	-3
			8.5	-81			12.5	-81.5
							7	-93
0.037 to 0.088 mm	2/5/66		68	0	2/5/66		128	+1
			24	0			58	+1.5
			21	-2.5			23	-7
		17.5	13	-75			19.5	-5
			8	-80		17.5	13	-96.5
							9	-90.5
≤ 0.037 mm	2/5/66		68	+2	2/5/66		128	+1
			26.5	-0.5			59	0
			22	-6.5			29	0
		18.5	13.5	-77.5			22	-1
			8.5	-83		18.5	11.5	-92
							7	-92
≤ 1μ	2/3/66		68	-2	2/3/66		128	-1.5
			33	-1			59	-2
			25	-7.5			29	-1
		23.0	18.5	-80.5			24	-0.5
			14	-86		23.0	15.5	-94
							12	-91.5

VOLCANIC ASH NO. 1

0.088 to 0.21 mm	2/7/66		68	0	2/7/66		128	0
			31	+0.5			58	-1
			26	-4.5			29.5	-2
		24.5	22	-77			27	+0.5
			15	-85.5		24.5	18	-101.5
							12	-92
≤ 1μ	2/8/66		68	+2.5	2/8/66		128	-3.5
			35	+1			58.5	-3
			28	-2.5			30	-3.5
		25.0	19	-83			25	-4
			11	-82		25.0	18	-95
			6.5	-82.5			9	-95

Table 2 (continued)

VOLCANIC ASH NO. 4

Particle Size	Zero Degree Polarimeter				60 Degree Polarimeter			
	Date	Inversion Angle	Phase Angle	ϵ_r	Date	Inversion Angle	Phase Angle	ϵ_r
2.83 to 6.35 mm	1/31/66		68°	+2°	1/31/66		128°	-2°
			40	+2			110	-2.5
		21.0°	24.5	-3			60	-2.5
			10	-86			40	-3.5
							30	-4
						21.0°	25	-7.5
							13	-94
1.19 to 2.83 mm	1/31/66		68	+1.5	1/31/66		128	-1
			40	+2			61	-0.5
			30	+0.5			40	0
			25	-3			30	-2
		21.5	13	-84.5			25	-1
						21.5	14	-90
0.50 to 1.19 mm	1/31/66		68	+1.5	2/1/66		128	+1
			40	+1.5			61	-0.5
			30	-1			39	+0.5
			25	-6.5			30	+1.5
		23.0	13	-86.5			26	+1.5
						23.0	13	-90
	1/31/66		68	-1.5				
			26	-1				
		23.0	20.5	-66				
			18	-86.5				
			15	-85.5				
0.21 to 0.50 mm	2/1/66		68	+2	2/1/66		128	-2
			24.5	-5			58	-1.5
		23.5	23	-19.5		23.5	23	-0.5
			21	-76.5			22.5	-3
			15.5	-87.5			19.5	-94.5
							14	-92 5
0.088 to 0.21 mm	2/2/66		68	+1.5	2/1/66		128	+1
			24	-2.5			58	-0.5
		22.5	22	-8.5			26.5	+1
			19.5	-78		22.5	22	-0.5
			12.5	-87.5			19.5	-88.5
							13	-93
0.037 to 0.088	2/2/66		68	-1	2/1/66		128	-2
			25	-0.5			55	-1
		22.5	22	-8.5			25	-1.5
			19	-66.5			23.5	+4.5
			14	-85		22.5	18	-87
							9	-89.5
≤ 0.037mm	2/2/66		68	+1	2/2/66		128	+0.5
			28	-1.5			61	+0.5
			22	-7.5			24.5	+1.5
		20.5	18.5	-75.5		20.5	20.5	0
			12.5	-83			18.5	-90
							15	-90
≤ 1μ	2/4/66		68	+0.5	2/4/66		128	-2.5
			29	-4			55	-3
			24	-4			31	-3.5
		24.0	16	-82		24.0	24	-8
			8.5	-86			17	-95
							11.5	-93.5

CORAL NO. 1

0.088 to 0.21 mm	2/9/66		68	0	2/9/66		128	-1
			36	-0.5			57.5	+1.5
			30	-6			33	0
		29.0	26	-7		29.0	8.5	-96
			10	-77.5				
			7	-71				
≤ 1μ	2/10/66		68	+4	2/9/66		128	0
			42	-2			59.5	+2
			30	+1			32	0
		27.5				27.5	27	+2.5
							7	+1

Table 2 (continued)

COPPER OXIDE

Particle Size	Zero Degree Polarimeter				60 Degree Polarimeter			
	Date	Inversion Angle	Phase Angle	δ_r	Date	Inversion Angle	Phase Angle	δ_r
0.088 to 0.21 mm	2/11/66		68°	+2.5	2/11/66		128°	-0.5
			39	+1.5			55	+0.5
			33	+0.5			35.5	-1.5
			27	-0.5			28	-3.5
		17.5°	19	-16.5		17.5°	20	-0.5
			12	-77.5			13	-89.5
			5.5	-78.5			6	-90
≤ 1μ	2/10/66		68	+1.5	2/10/66		128	-1.5
			23	-1.5			57	-4
		14.5	18	-5			27	-4
			10	-69.5		14.5	20.5	-5.5
			6	-70.5			5	-90.5

SILVER CHLORIDE

0.088 to 0.210 mm	2/2/66		68	+1.5	2/12/66		128	0
			38	0			56	-0.5
		15.0	19	-4.5			32	-3
			10	-50.5		15.0	20	-2
			5	-78.5			12.5	-87
							5	-93.5
3-8μ	2/12/66		68	+3	2/12/66		128	-2.5
			35	0			57	-2.5
		17.0	20	-6.5			25	-3.5
			15	-12.5		17.0	18	-4.5
			8	-70.5			10	-88
							5	-92
≤ 1μ	2/14/66		68	+1	2/14/66		128	+1
			28	-9.5			55	-1
		26.5	23.5	-14			36.5	-1
			18.5	-72		26.5	30	-2.5
			13	-82.5			16	-98.5
							5	-95.5

4. On observations at phase angles below the inversion, there is an apparent wandering of the position of the plane of polarization from 90°; this is fundamentally the result of the low signal to noise ratio because of the small amount of polarization (negative) below inversion.

The lunar data of Gehrels et al. (Ref. 8) and the laboratory sample data of Coffeen (Ref. 13) do not clearly show a trend in the position of the plane of polarization with phase angle. We cannot definitely determine whether the plane of polarization continuously changes from 0° to 90° as the inversion angle is passed, as seen by the Russian observers (see Ref. 9). Their observations appear to be the result of an instrumental effect, and from our data, this effect cannot be determined.

Lunar Implications

On the basis of data obtained for the percent polarization of the various samples as a function of phase angle (summarized in Table 1), we may infer the appropriateness of particular samples as possessing properties characteristic of the lunar surface. At the bottom of Table 1 are summarized the properties of Mare Crisium and Clavius as well as the Lyot average curve. In addition, the Mare Crisium and Clavius curves are presented as comparison data in Figs. 5 through 27.

For Furnace Slag No. 4 (Fig. 15) the Mare Crisium curve is fitted best for particle sizes below 37 microns, Clavius for particle sizes below 1 micron. This assumes that one particle size alone exists in these areas, which is probably far from true. But the general trend does indicate that smaller particles fit the highland curves best.

Volcanic Ash No. 4 (Fig. 8) shows the same trend, but the particle sizes are larger, possibly the result of the lower density of the volcanic ash as compared to the furnace slag. Mare Crisium is best fit by particles between 37 and 88 microns, and Clavius by particles between about 37 microns and 1 micron.

Volcanic Ash No. 1 (Fig. 23) appears to require particles greater than the 0.088 to 0.21 mm range to match Mare Crisium, possibly because of the lighter color of our sample as compared to the material in the maria; a match to Clavius appears to necessitate particles less than 1 micron in size.

Copper oxide (Fig. 21), coral (Fig. 19) and silver chloride (Fig. 20) alone are unsatisfactory because of maximum polarization well out of the range required to simulate the lunar surface.

The Vesuvius Cinders (Fig. 25) match the Mare Crisium lowlands curve fairly closely, which is a rather interesting analogy considering the origin of the cinders.

The sponge-like slag (Fig. 27) obtained at NASA/MSC appears to offer some possibility as a lunar simulator, because it would only require a moderate modification of the polarization characteristics with a surface coating to match Mare Crisium; the maximum polarization would have to be diminished, the corresponding phase angle reduced to about 102 degrees, and the inversion shifted to about 23.7 degrees. This might be approximated by coating it with Furnace Slag No. 4 particles less than 1 micron. This, as well as color implications, will be investigated more completely in Phase III.

The Vesuvius Cinders appear to show greater promise if the polarization peak could be shifted to a smaller angle by combining the cinders with a nonpolarizing material of varying albedo. This too will be investigated in Phase III.

The effect of proton bombardment could alter the results observed on the powders (Refs. 11 and 12). It could conceivably change the results observed on the bulk samples of Vesuvius Cinder and Furnace Slag.

Our observed results on Volcanic Ashes are in agreement with those shown by Coffeen (Ref. 13) for a Fairy-Castle structure of Volcanic Ash. Thus, the G_1 polarization observed by Coffeen increases from 6 to 11 percent as the average particle size is decreased from 3 to 1 mm. In Fig. 7, it is observed that as the particle size goes from the 2.83 to 6.35mm range to 0.5 to 1.19mm range, the polarization increases from 16.6 to 18.1 percent.

The albedo-polarization data summarized in Fig. 29 for Furnace Slag No. 4 and Volcanic Ash Nos. 1 and 4 yield additional information; the two straight lines show the appropriate trends for the Furnace Slag and the Volcanic Ashes. The difference in the two curves might be the result of the higher real density of the Furnace Slag above the Volcanic Ashes. Two lunar points from Gehrels et al. (Ref. 8) used in the present data analysis are shown; the Mare Crisium point lies on the Volcanic Ash curve, while the Clavius point is above both curves.

A comparison is made to the proton bombardment data of Wehner et al. (Ref. 12). The Wehner data for 74 to 300μ tholeiitic basalt and 44 to 74μ granodiorite are shown. These lie on the upper extreme of the Wehner data, with smaller particles lying below the curves; this is also true for 74 to 300μ tektite and 74 to 300μ greenstone. Wehner had used the Russian lunar data to compare with the laboratory polarization-albedo data. It is felt that the Russian lunar data is inaccurate and Gehrels' data more accurate (see Ref. 9). Thus, one would infer that bombarded particles of these materials having a size of about 74 to 300 microns would fit the lunar data best. This is larger than the range of sizes obtained from the present study.

The data on silver chloride, copper oxide, and coral were not plotted on the graph because it was felt that they were not representative of typical lunar surface data.

CONCLUSIONS

As a result of Phase II, we have delimited the range of particle sizes that would have to exist on the lunar surface, either as a contiguous volume or as a simple, thin layer of the order of up to 1 mm thickness. This model is consistent with the Luna 9 observations, and also with the thermophysical and photometric models analyzed at Grumman (Refs. 3, 4, and 6). It must also be remembered that the present observations are made under terrestrial conditions, and the high vacuum conditions on the moon plus the effect of solar wind proton bombardment could possibly alter the results.

Even though closely defined ranges of particle sizes were used in this investigation, one would not assume that these specific ranges exist on the lunar surface to give the observed polarization. The particle ranges observed in this work serve as guides in correlating photometric, polarization, and thermophysical data.

The nonuniqueness of a surface contrived to give an observed polarization must still be emphasized, although guides to a proper configuration evolve from a consideration of all available data.

It appears that the polarization - albedo - porosity relationship for the particles below 0.5 mm in size may be used to advantage in elucidating the mechanical properties as well as the thermal properties of a lunar surface model (Ref. 14).

The work of Phase III may yield additional surface information based on color effects in polarization.

RECOMMENDATIONS

Useful areas for further investigation appear to be primarily in data interpretation. From the theoretical work pursued at Grumman to date, it appears that the experimental elucidation of data interpretation will precede the theory because of the extreme mathematical difficulties involved.

Some preliminary experimental work has already been done in the examination of the depolarization of a surface to find out the extent of multiple scattering, diffraction, refraction, and reflection.

Some areas that should be investigated are:

1. Theoretical correlation of albedo and maximum percent polarization.

2. Effect of complex index of refraction of the materials on the inversion angle and negative maximum.

3. Extent and effect of multiple scattering, resulting in cross polarization or depolarization.

4. Effect of lunar luminescence on polarization, and observations of this luminescence directly.

5. Clarification of the discrepancy between our observations and the theoretical curve of Hapke (Ref. 10).

6. Effect of proton bombardment on large scale samples.

7. Investigation of different parameters (other than maximum and minimum polarization with corresponding angles, and inversion angle) to specify polarimetric curves (i.e., "Polarization Rise" - Ref. 12).

REFERENCES

1. Egan, W. G. and Smith, L. L., Polarimetric Measurements of Simulated Lunar Surfaces, Grumman Research Department Memorandum RM-304, First Progress Report on NASA Contract No. NAS 9-4942, December 1965.

2. New York Times, February 6, 1966, "Moscow Releases 2 of Its Moon Photos," p. 1.

3. Halajian, J. D. Photometric Measurements of Simulated Lunar Surfaces, Grumman Research Department Report RE-219, Interim Report on NASA Contract No. NAS 9-3182, July 1965.

4. Halajian, J. D. and Spagnolo, F. A., Photometric Measurements of Simulated Lunar Surfaces, Grumman Research Department Memorandum RM-308, Quarterly Progress Report on NASA Contract No. NAS 9-3182, January 1966.

5. Strom, R. G., Private communication.

6. Halajian, J. D. and Reichman, J., Correlation of Mechanical and Thermal Properties of Extraterrestrial Materials, Grumman Research Department Memorandum RM-309, February 1966.

7. Lyot, B., "Research on the Polarization of Light from Planets and Some Terrestrial Substances," Annales de l'Observatorie de Paris, Section de Meudon, 8, No. 1, 1929, NASA Technical Translation: NASA TT F-187.

8. Gehrels, T., Coffeen, T., and Owings, D., "Wavelength Dependence of Polarization, III. The Lunar Surface," Astronomical Journal, 69, No. 10, December 1964, pp. 826-852.

9. Egan, W. G., Polarimetry and the Lunar Surface - A Literature Survey, Grumman Research Department Memorandum RM-271, April 1965.

10. Hapke, B., Some Comments on Gehrels' Model of the Lunar Surface, Center for Radiophysics and Space Research Report CRSR 199, Cornell University, June 1965.

11. Hapke, B., Effects of a Simulated Solar Wind on the Photometric Properties of Rocks and Powders, Center for Radiophysics and Space Research Report CRSR 169, Cornell University, June 1964.

12. Wehner, G. K., Rosenberg, D. L., and Ken Knight, C. E., Investigation of Sputtering Effects on the Moon's Surface, Eighth Quarterly Status Report on Contract No. NASw-751, Report No. 2792, May 14, 1965, Applied Science Division, Litton Systems, Inc., Minneapolis, Minnesota.

13. Coffeen, D. L., "Wavelength Dependence of Polarization. IV. Volcanic Cinders and Particles," Astronomical Journal, 70, No. 6, August 1965, pp. 403-413.

14. Halajian, J. D., "The Case for a Cohesive Lunar Surface Model," Annals of the New York Academy of Sciences, 123, Art. 2, July 15, 1965, pp. 671-710.

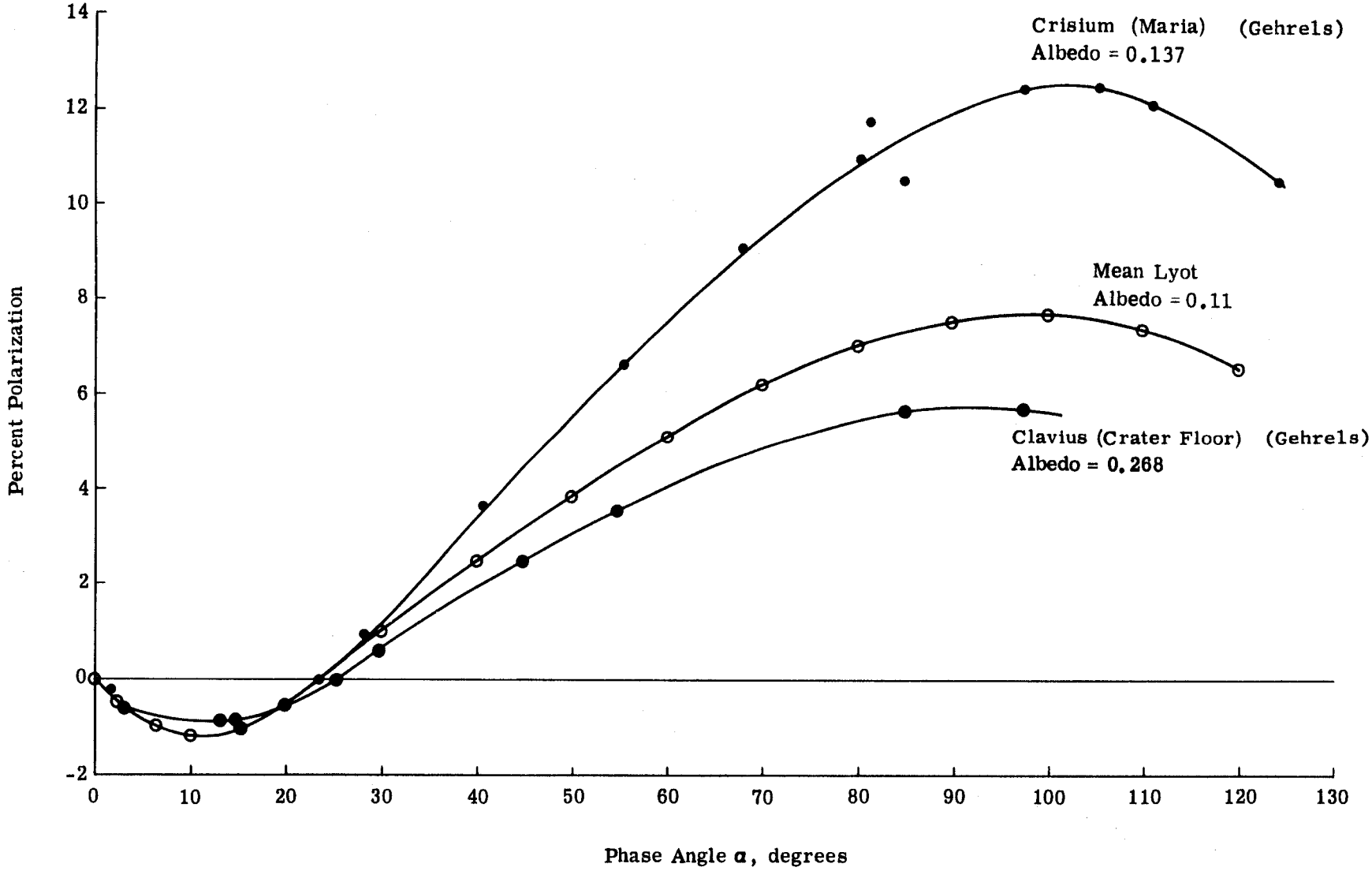

Fig. 1 Polarization Curves of the Moon

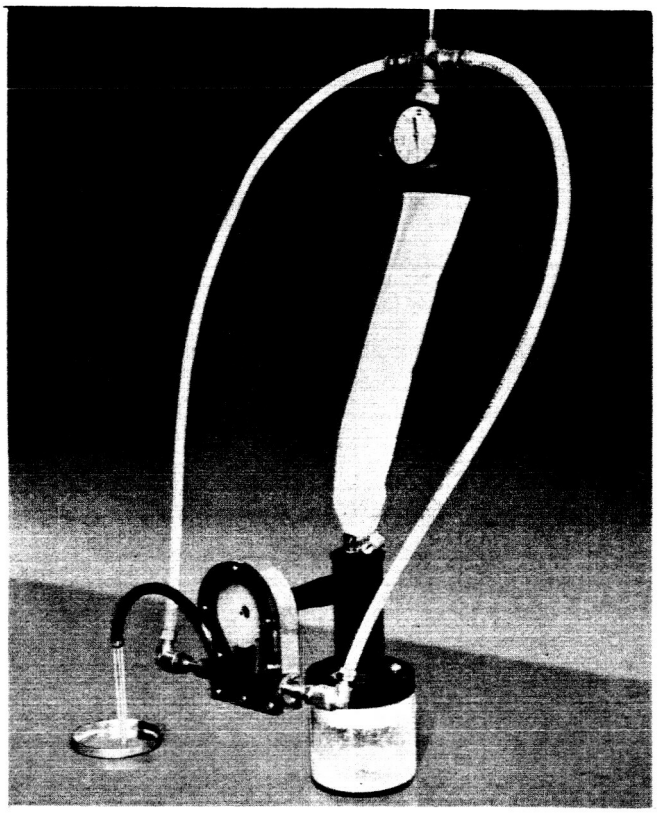

Fig. 2 Helme Fluid Energy Mill Assembly

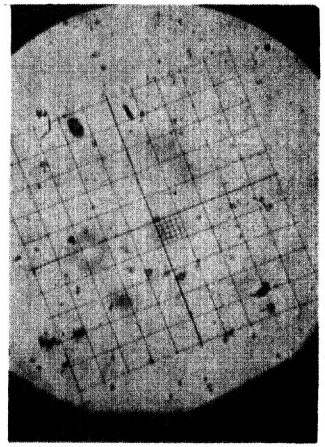

a) Volcanic Ash #4
25μ/div ≤ 1μ (1-17-66)

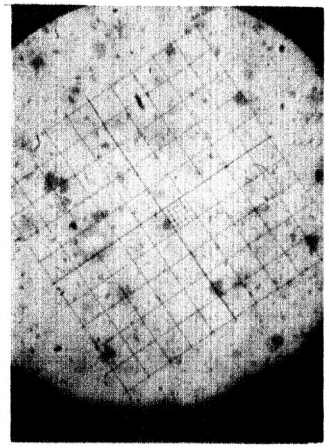

b) Furnace Slag #4
25μ/div ≤ 1μ (1-18-66)

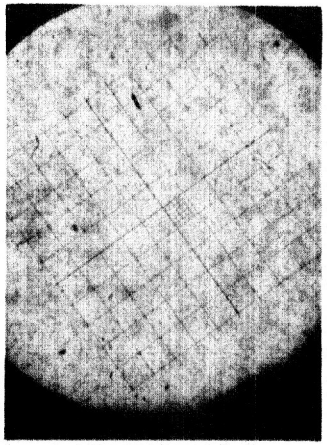

c) Volcanic Ash #1
25μ/div ≤ 1μ (1-18-66)

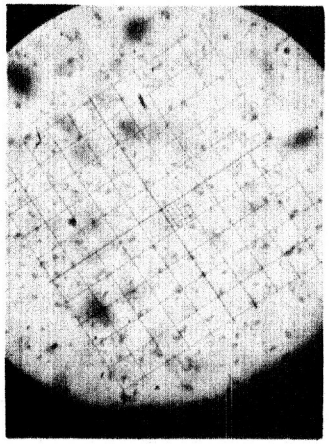

d) Copper Oxide
25μ/div ≤ 1μ (1-18-66)

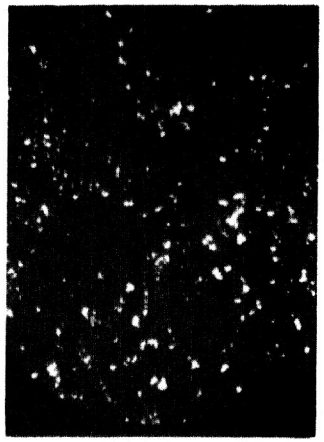

e) Silver Chloride
Precipitate
25μ/div < 1μ (2-10-66)
(Dark Field Illumination)

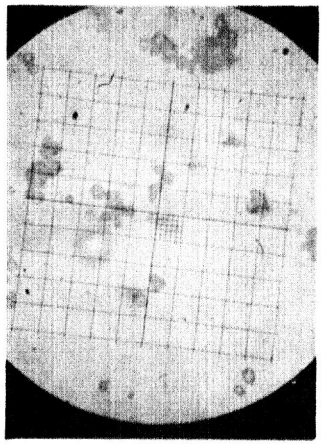

f) Silver Chloride
Fluid Energy Mill Grind
12.5μ/div 3-8μ (2-10-66)

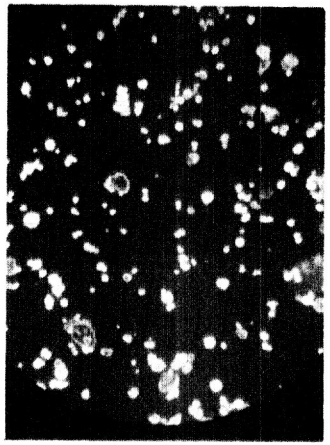

g) Silver Chloride
Fluid Energy Mill
25μ/div 3-8μ (2-10-66)
(Dark Field Illumination)

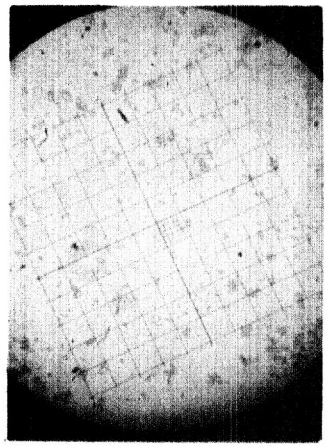

h) Coral #1
12.5μ/div ≤ 1μ (1-14-66)

Fig. 3 Microscope Photographs of Submicron Specimens Used in Polarimetric Investigation

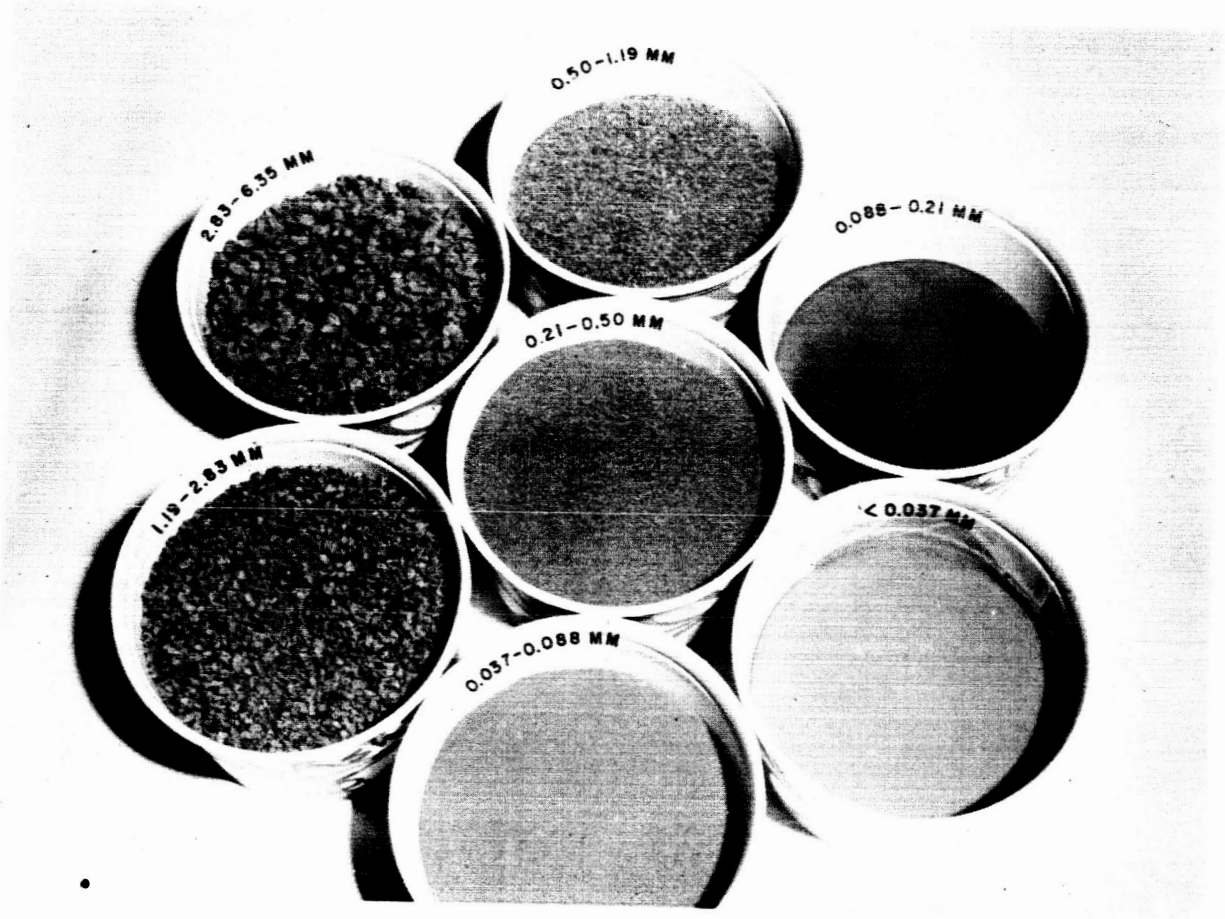

Ash No. 4, Ground and Sorted

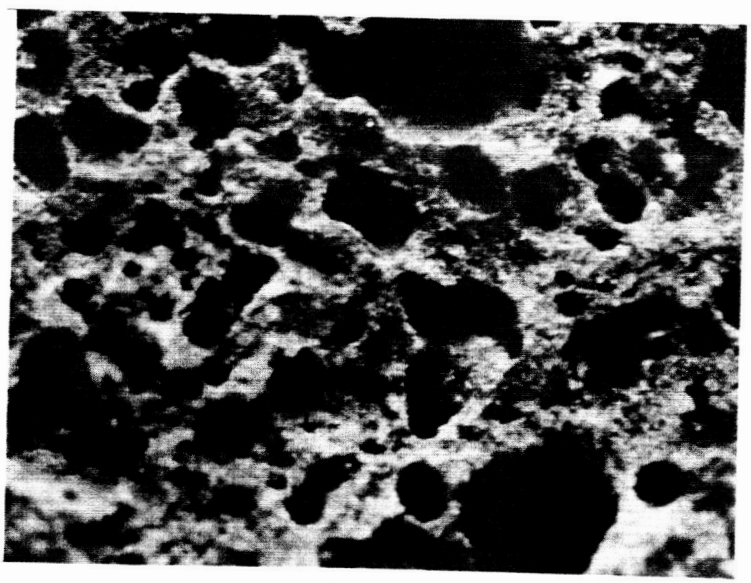

(a) 2.83-6.35 mm

Fig. 4 Polarimetry of Volcanic Ash No. 4 as a Function of Particle Size, Porosity, and Albedo

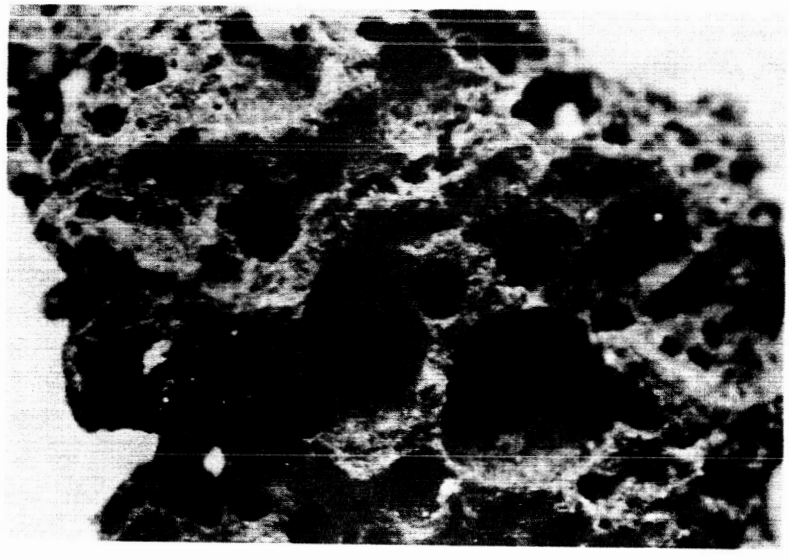

(b) 1.19-2.83 mm

(c) 0.50 to 1.19 mm

Fig. 4 (Cont.) Polarimetry of Volcanic Ash No. 4 as a Function of Particle Size, Porosity and Albedo

(d) 0.21 to 0.50 mm

(e) 0.088 to 0.21 mm

Fig. 4 (Cont.) Polarimetry of Volcanic Ash No. 4 as a Function of Particle Size, Porosity and Albedo

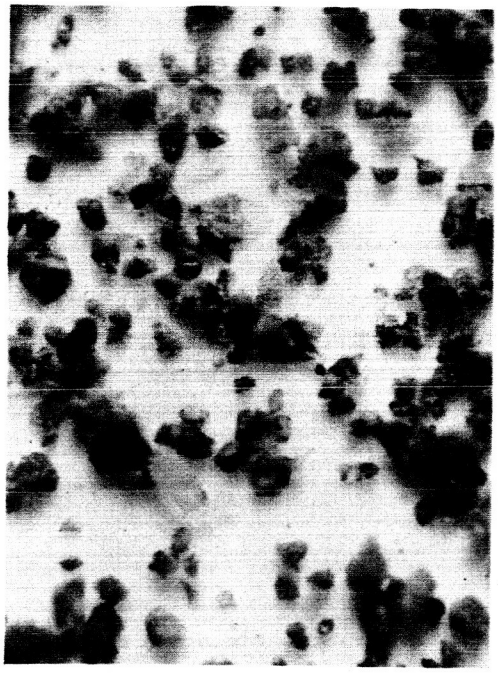

(f) 0.037 to 0.088 mm

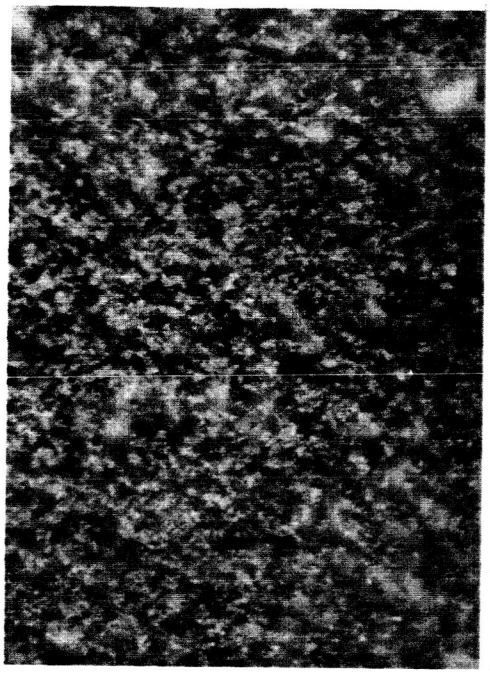

(g) $\leq$ .037μ

Fig. 4 (Cont.) Polarimetry of Volcanic Ash No. 4 as a Function of Particle Size, Porosity and Albedo

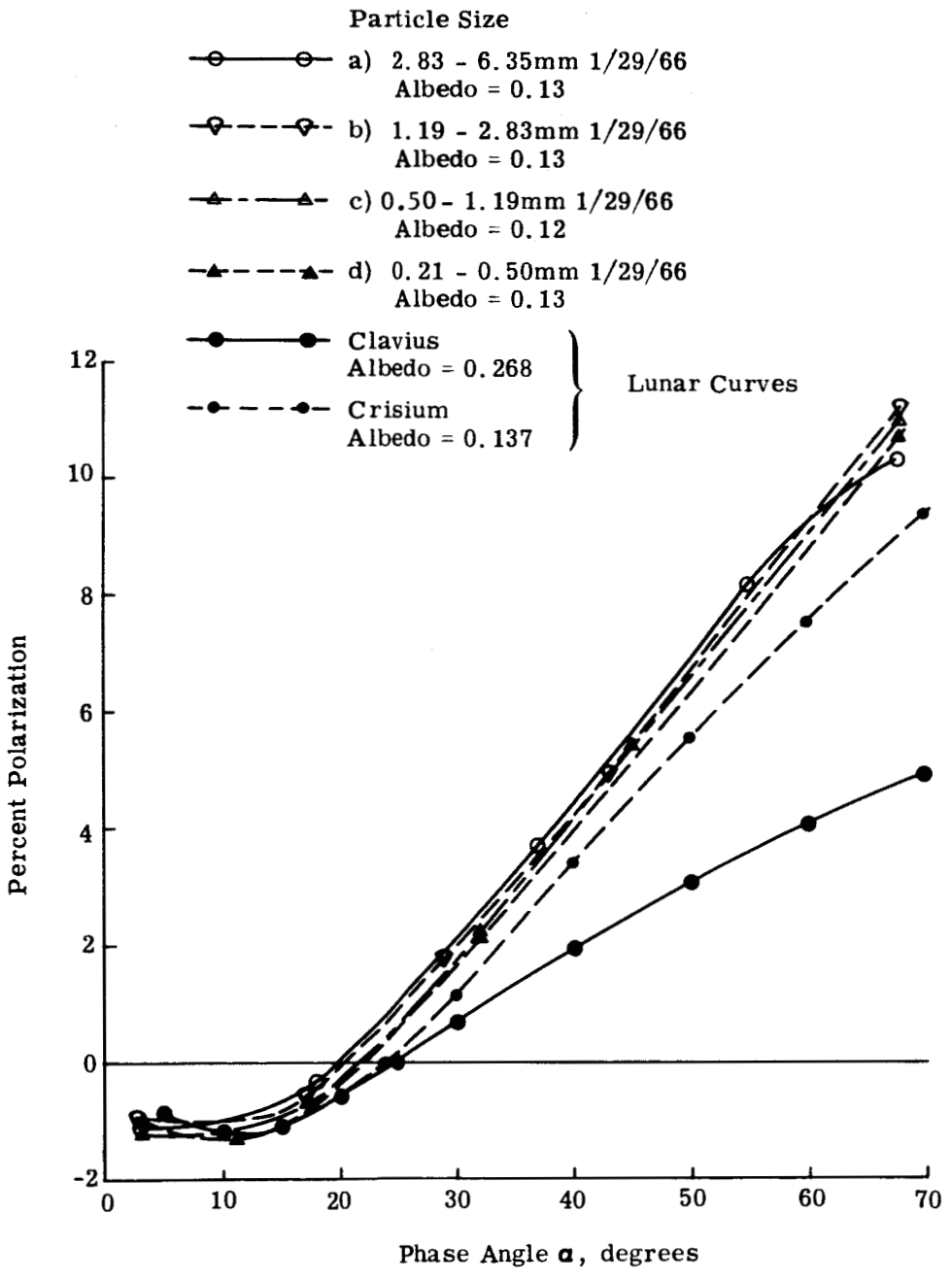

Fig. 5 Volcanic Ash No. 4: Percent Polarization as a Function of Particle Size for Largest Particles (Uncorrected for Instrumental Effect) - 0° Polarimeter

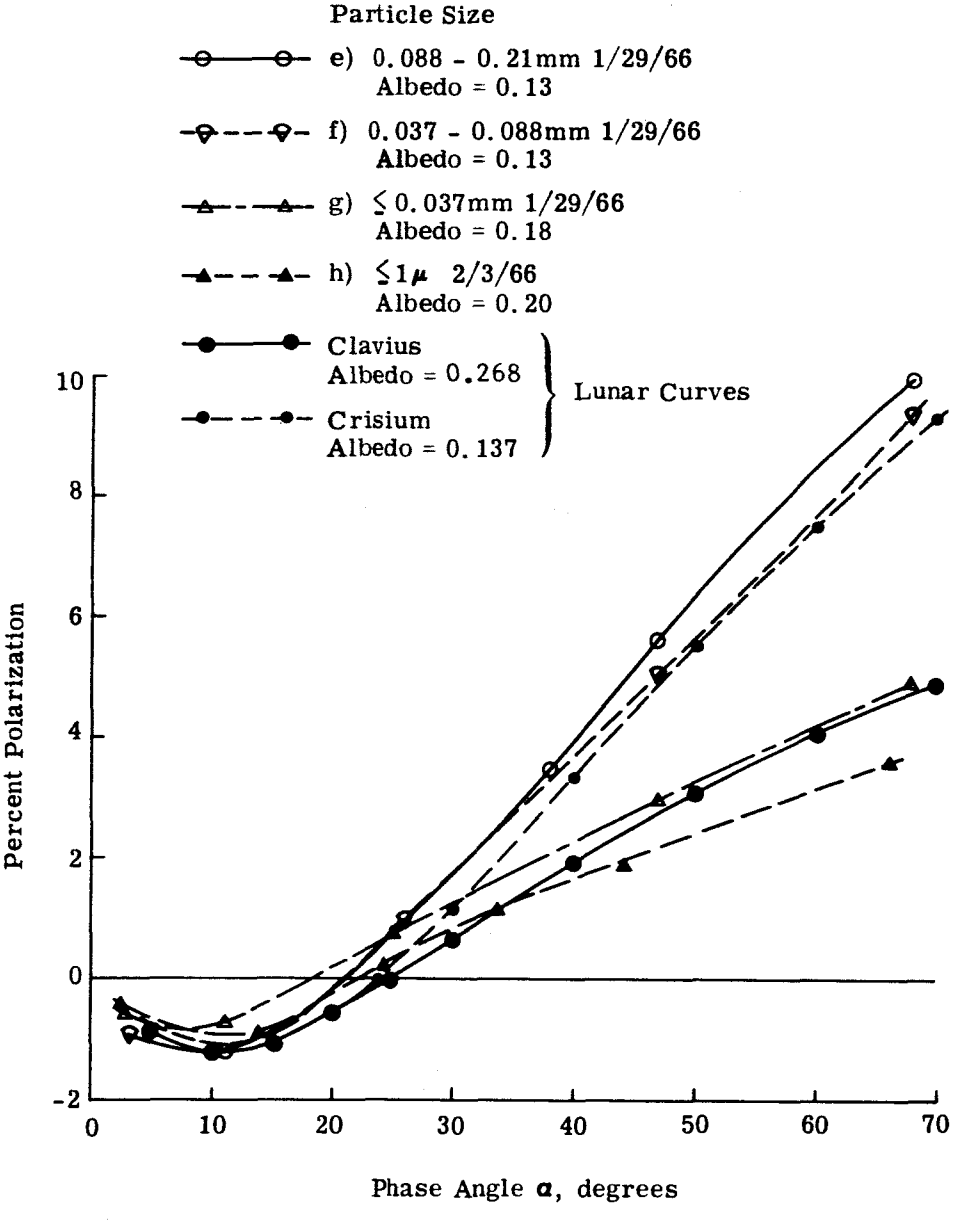

Fig. 6 Volcanic Ash No. 4: Percent Polarization as a Function of Particle Size for Smallest Particles (Uncorrected for Instrumental Effect) 0° Polarimeter

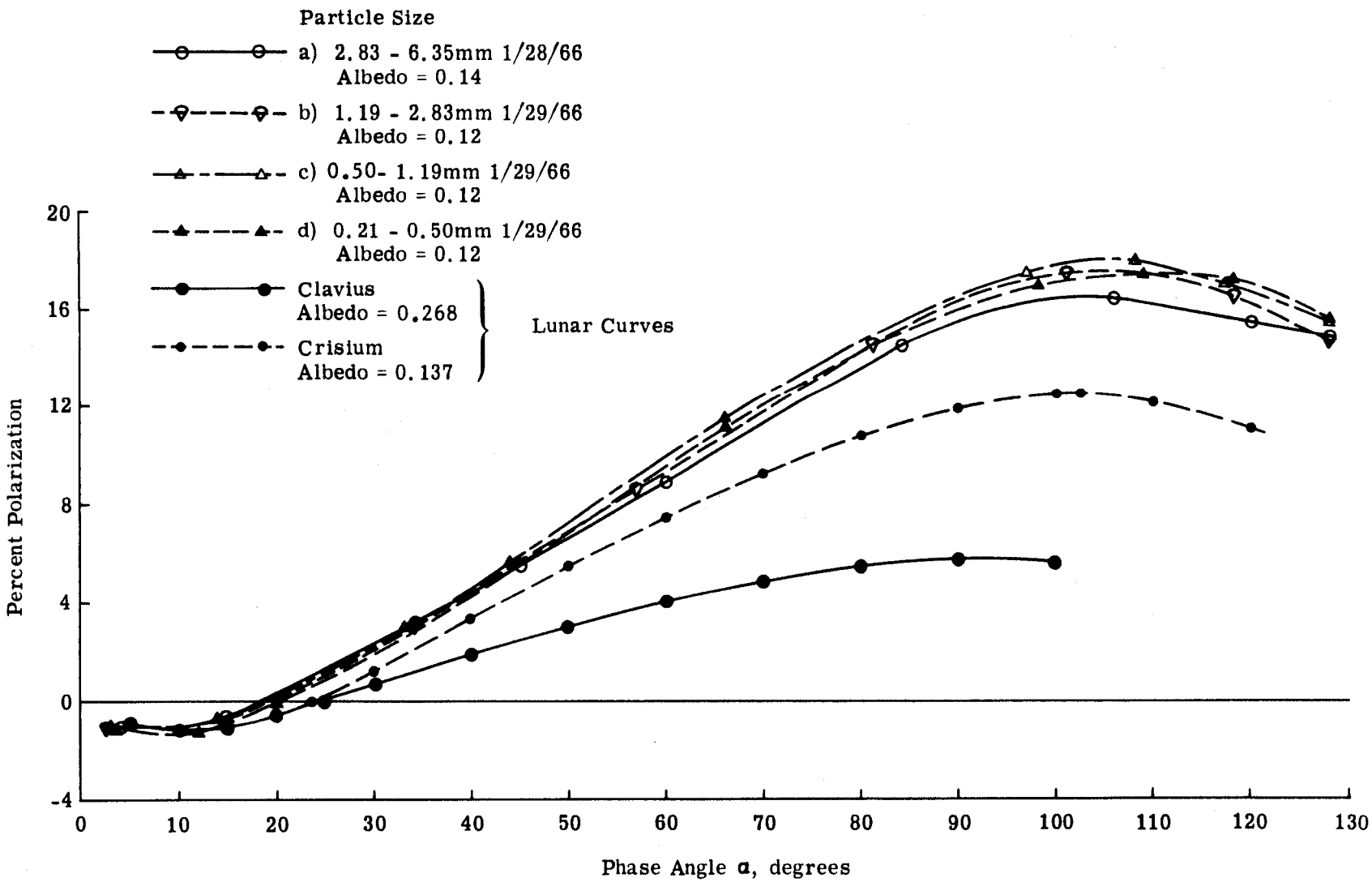

Fig. 7 Volcanic Ash No. 4: Percent Polarization as a Function of Particle Size for Largest Particles (Uncorrected for Instrumental Effect) 60^{o} Polarimter

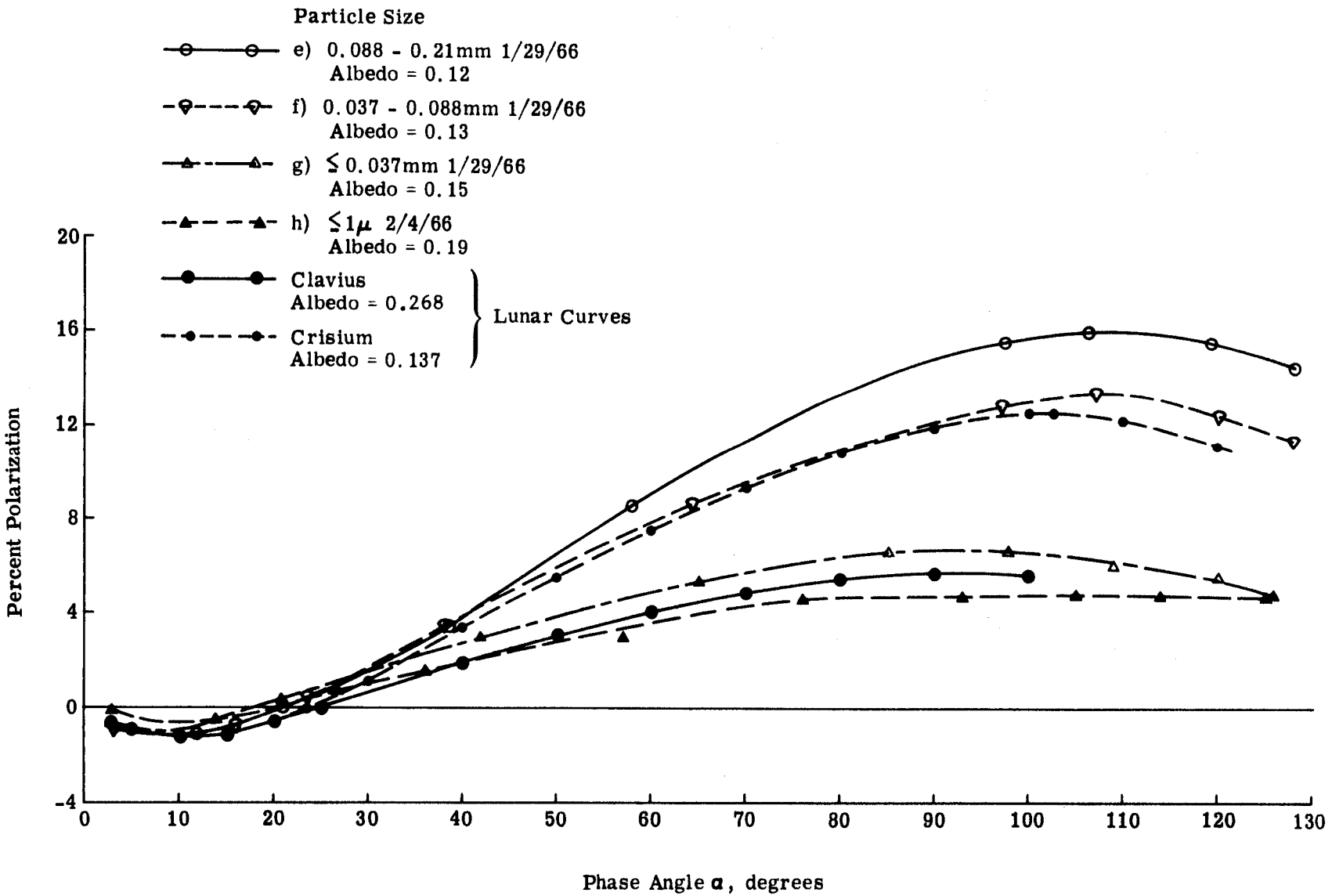

Fig. 8 Volcanic Ash No. 4: Percent Polarization as a Function of Particle Size for Smallest Particles (Uncorrected for Instrumental Effect) 60° Polarimeter

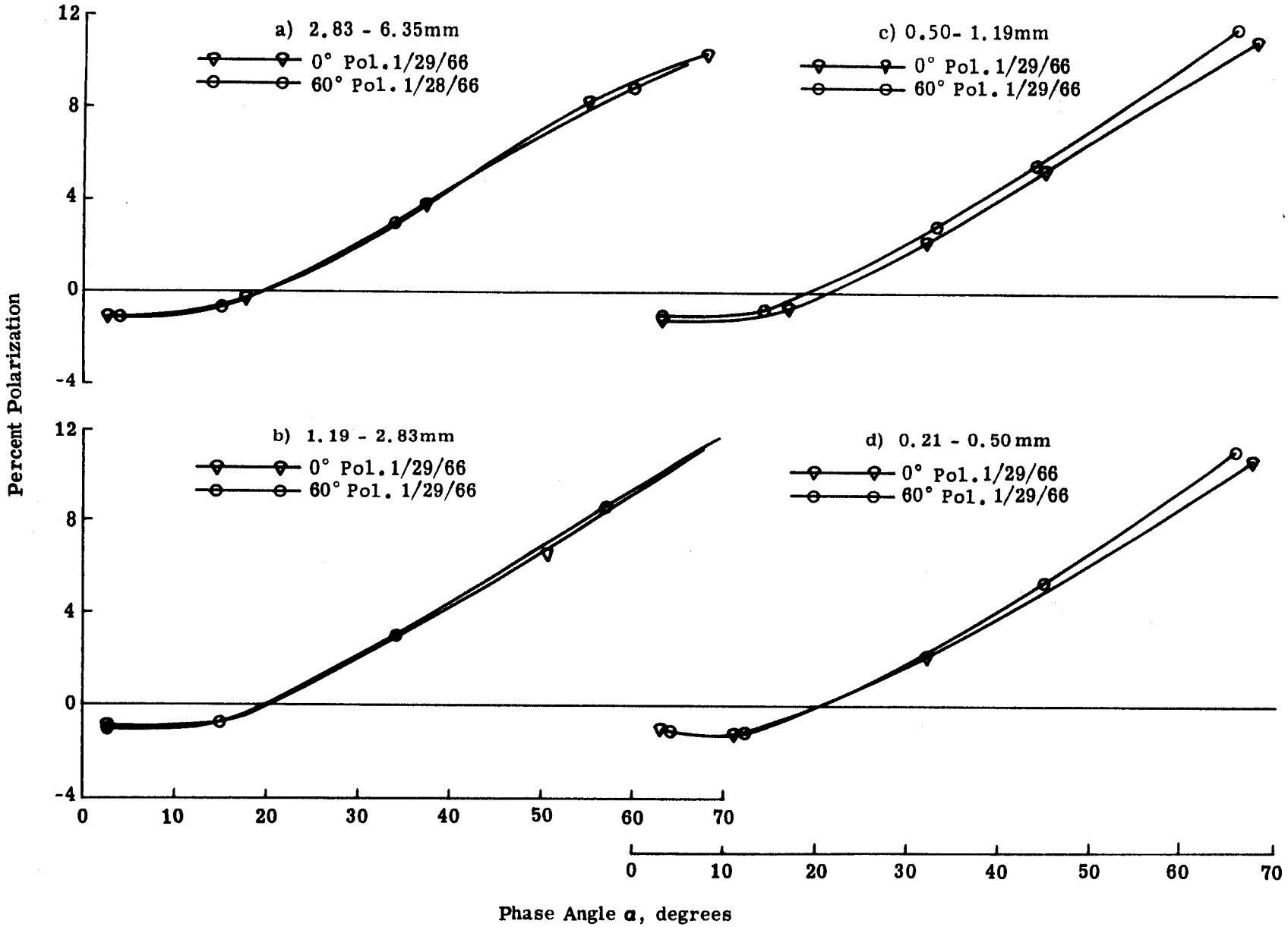

Fig. 9 Volcanic Ash No. 4: Simulated Lunar Longitude Effect on Percent Polarization for Largest Particles (Uncorrected for Instrumental Effect)

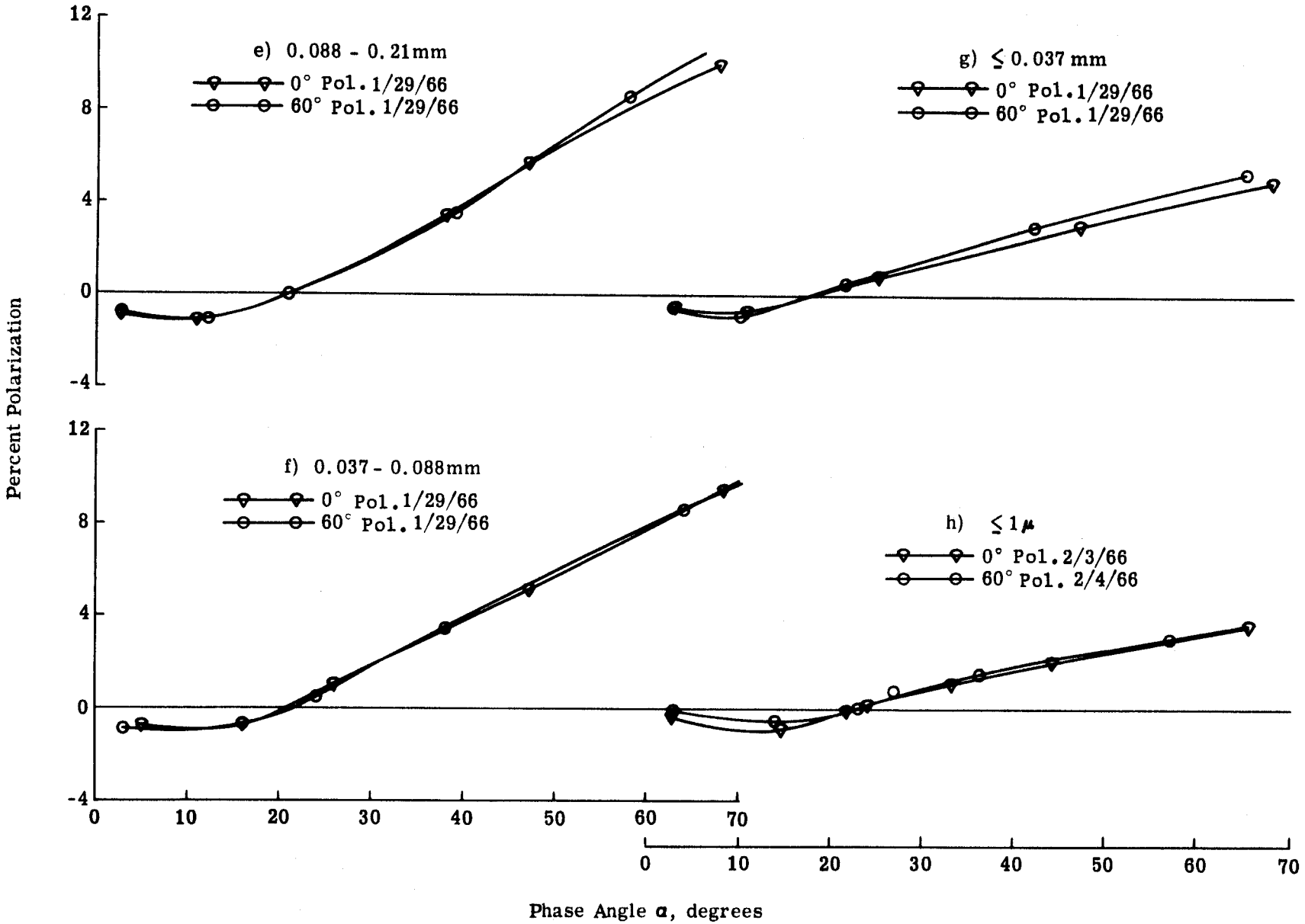

Fig. 10 Volcanic Ash No. 4: Simulated Lunar Longitude Effect on Percent Polarization for Smallest Particles (Uncorrected for Instrumental Effects)

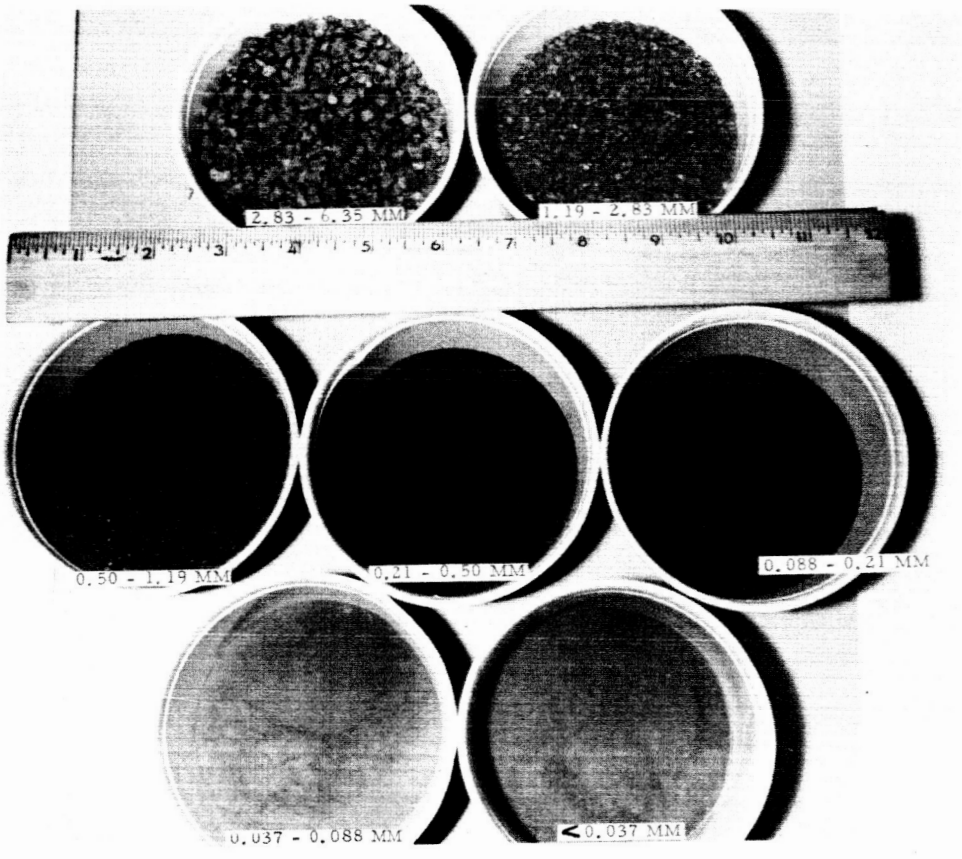

Fig. 11 Polarimtery of Furnace Slag No. 4 as a Function of Particle Size, Porosity, and Albedo

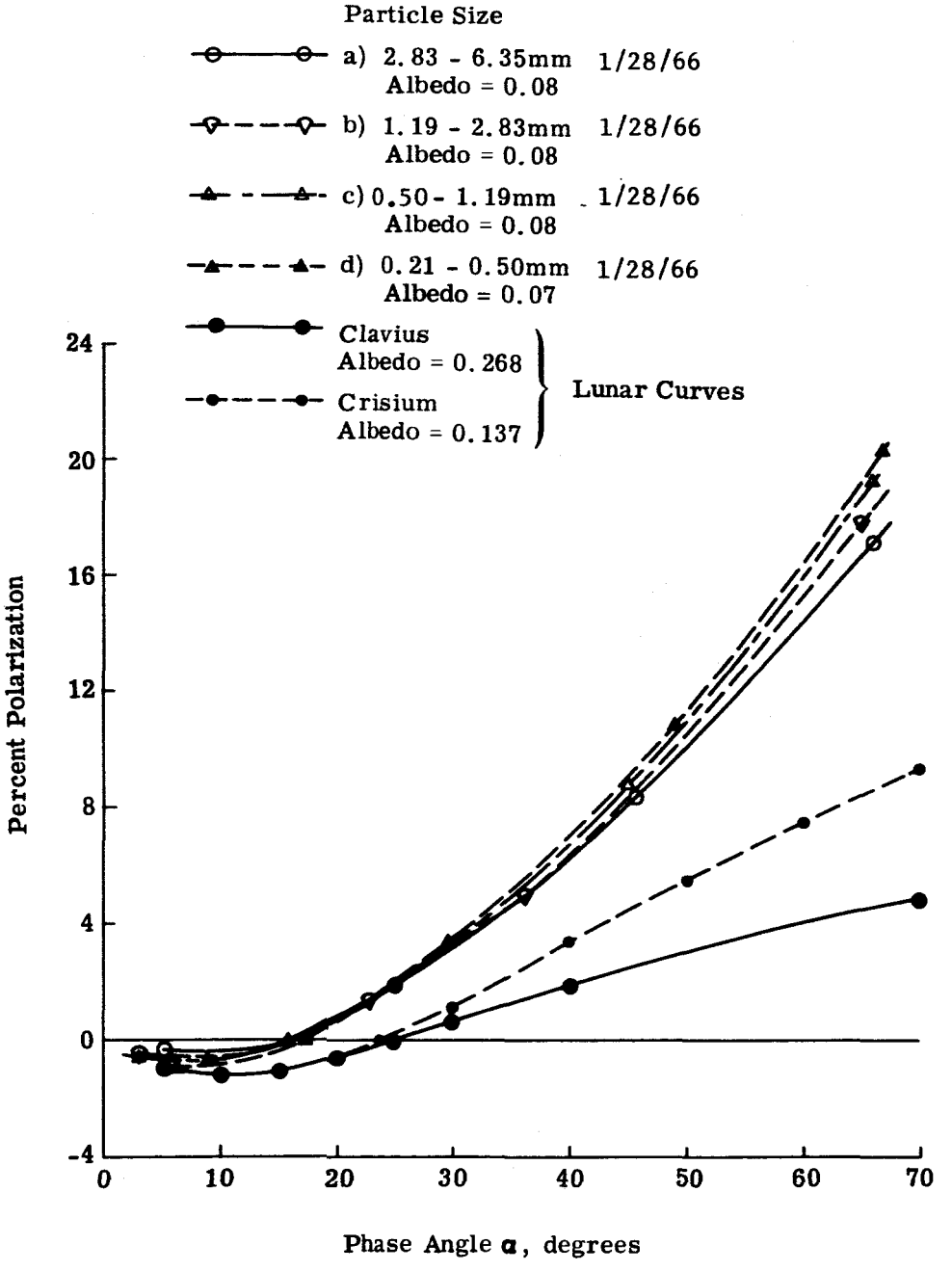

Fig. 12 Furnace Slag No. 4: Percent Polarization as a Function of Particle Size for Largest Particles (Uncorrected for Instrumental Effects) 0^{o} Polarimter

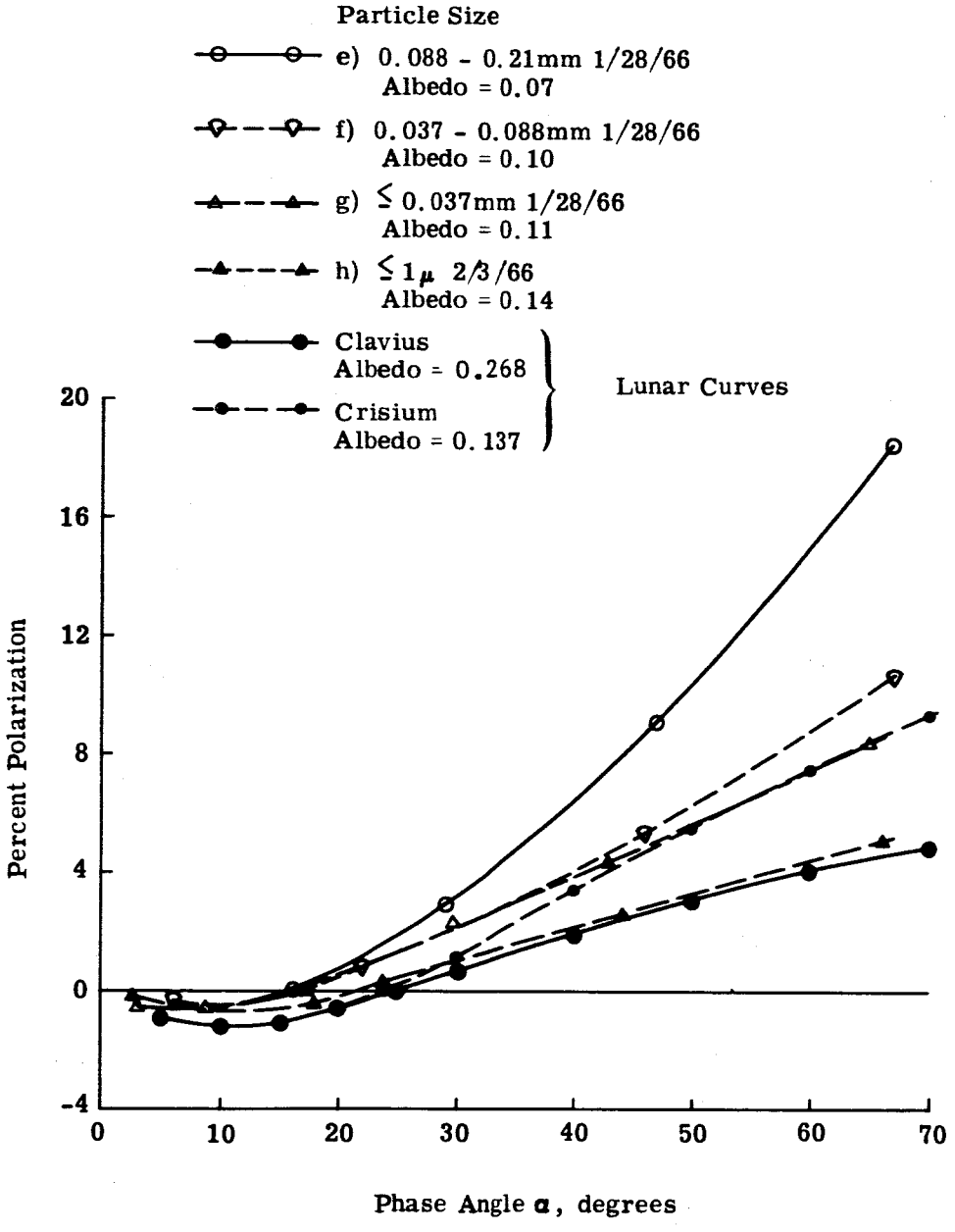

Fig. 13 Furnace Slag No. 4: Percent Polarization as a Function of Particle Size for Smallest Particles (Uncorrected for Instrumental Effects) 0^{o} Polarimter Polarimeter

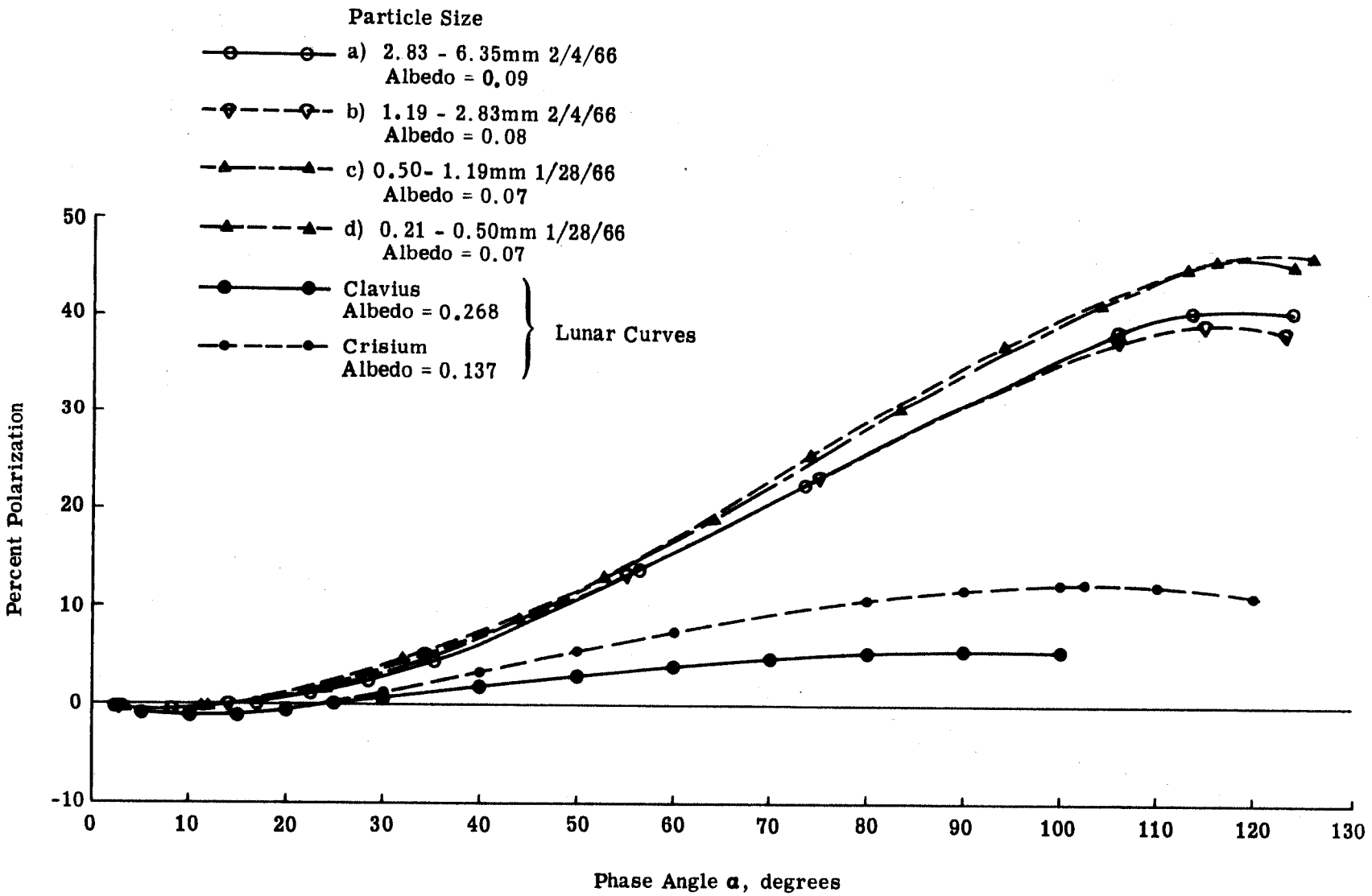

Fig. 14 Furnace Slag No. 4: Percent Polarization as a Function of Particle Size for Largest Particles (Uncorrected for Instrumental Effects) 60° Polarimeter

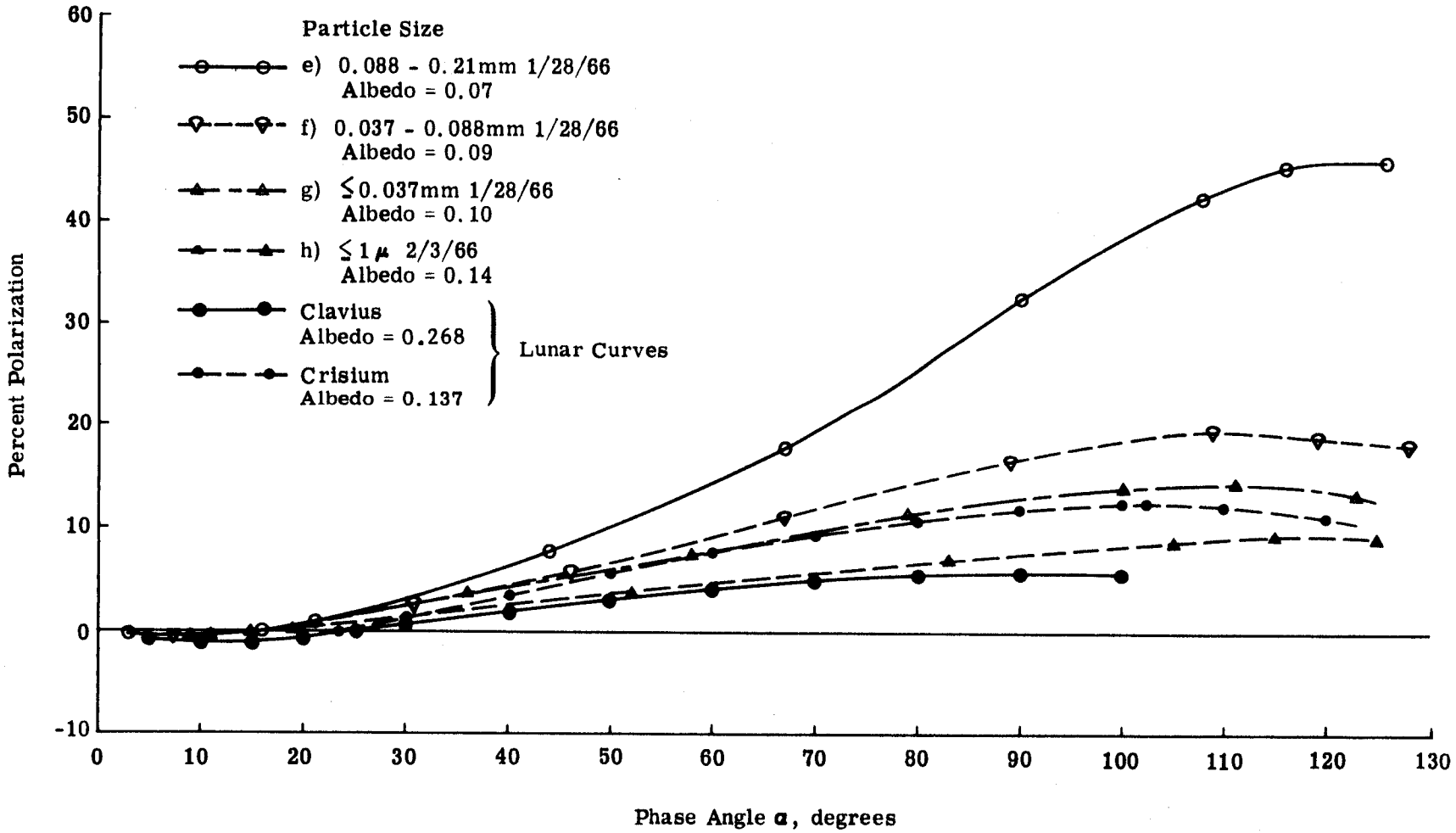

Fig. 15 Furnace Slag No. 4: Percent Polarization as a Function of Particle Size for Smallest Particles (Uncorrected for Instrumental Effects) 60° Polarimeter

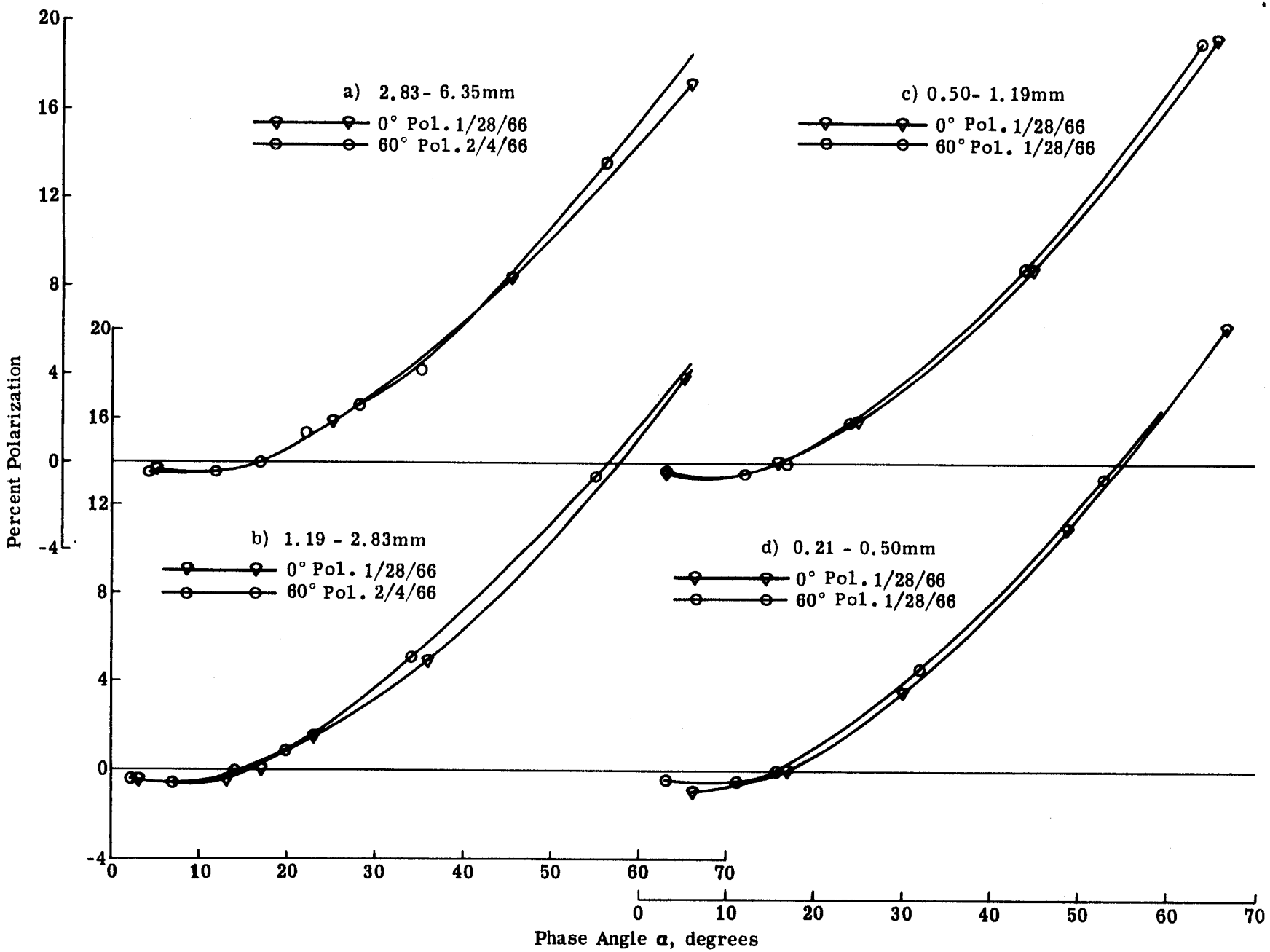

Fig. 16 Furnace Slag No. 4: Simulated Lunar Longitude Effects on Percent Polarization for Largest Particles (Uncorrected for Instrumental Effects)

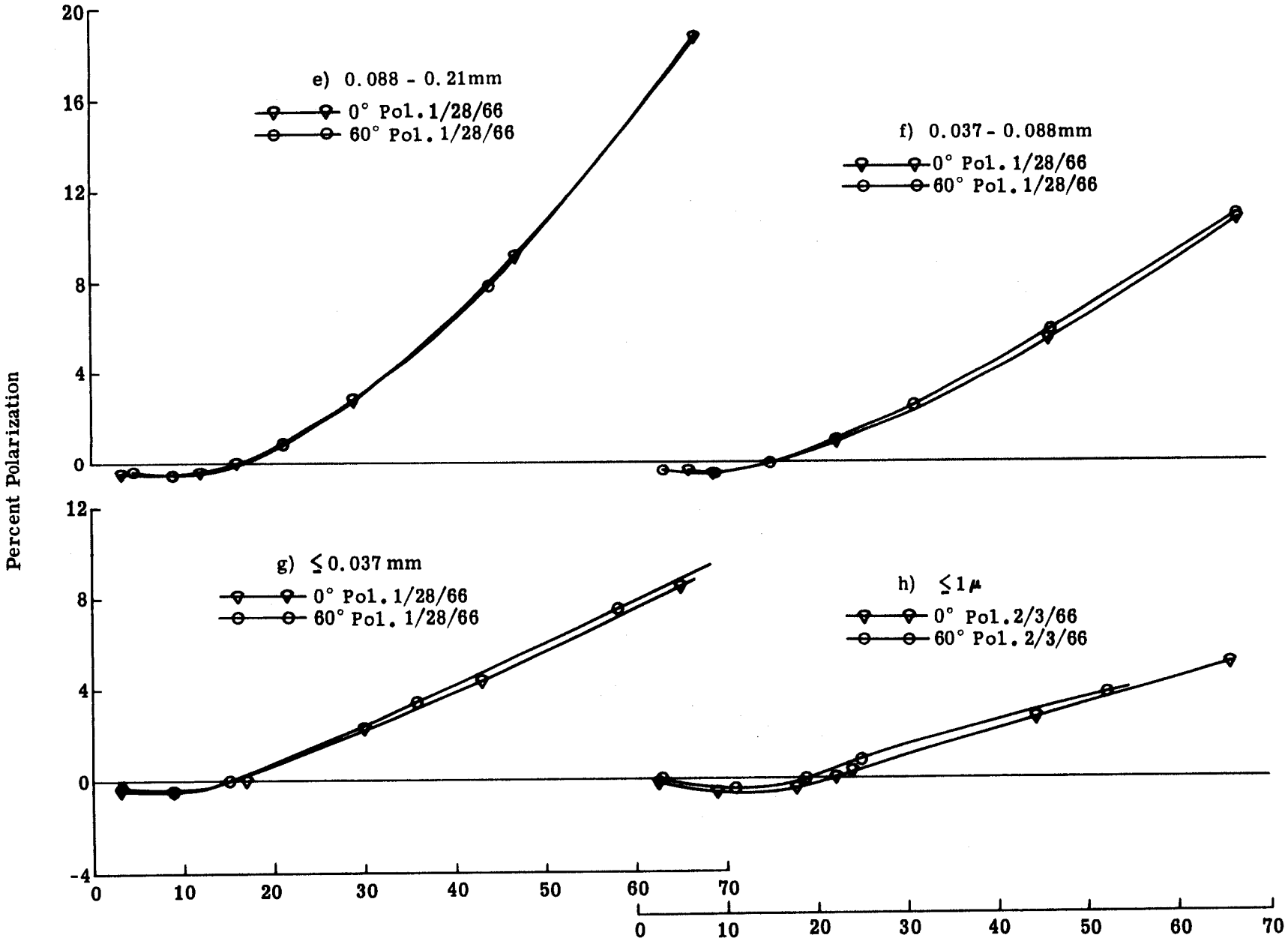

Fig. 17 Furnace Slag No. 4: Simulated Lunar Longitude Effects on Percent Polarization for Smallest Particles (Uncorrected for Instrumental Effects)

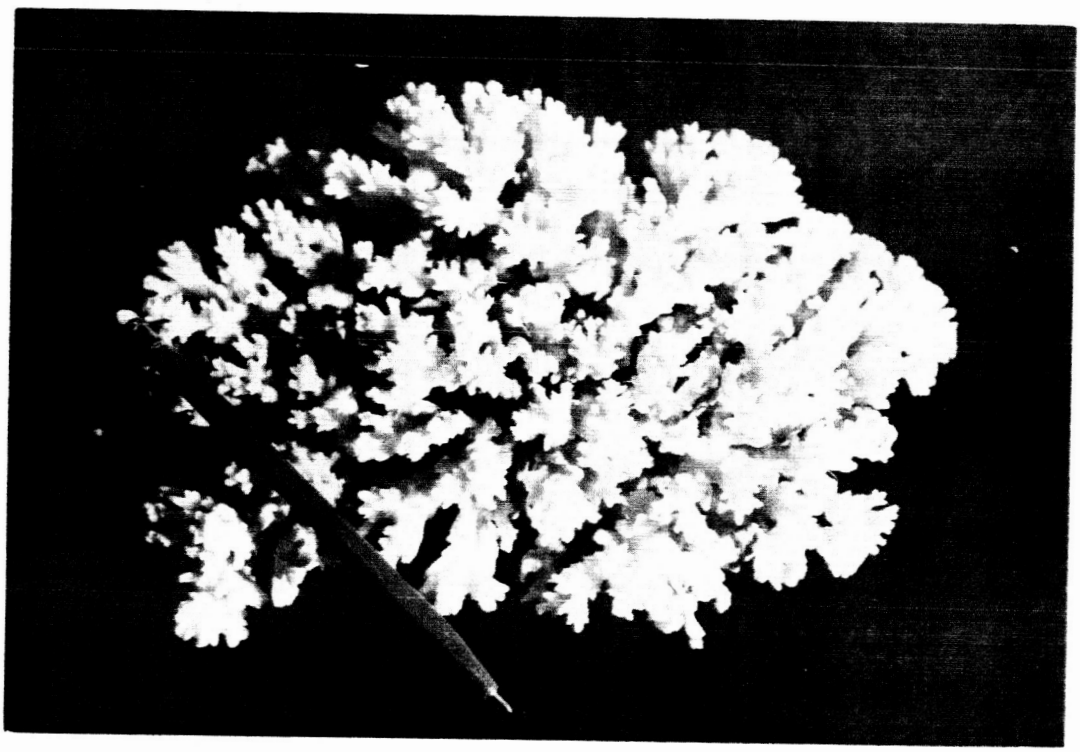

Fig. 18 Coral No. 1 (Unpulverized)

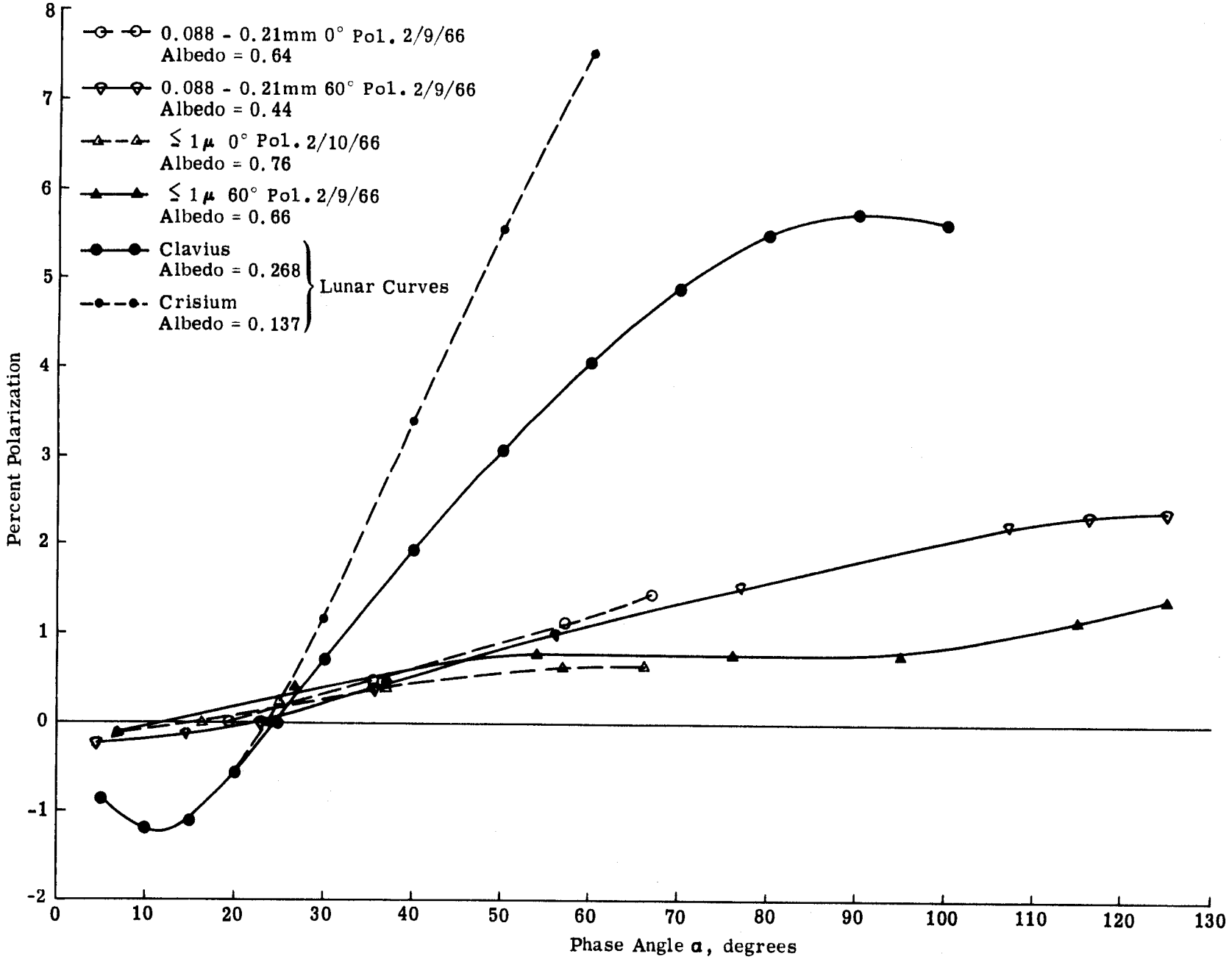

Fig. 19 Coral No. 1: Percent Polarization as a Function of Particle Size (Uncorrected for Instrumental Effects) 0° and 60° Polarimeters

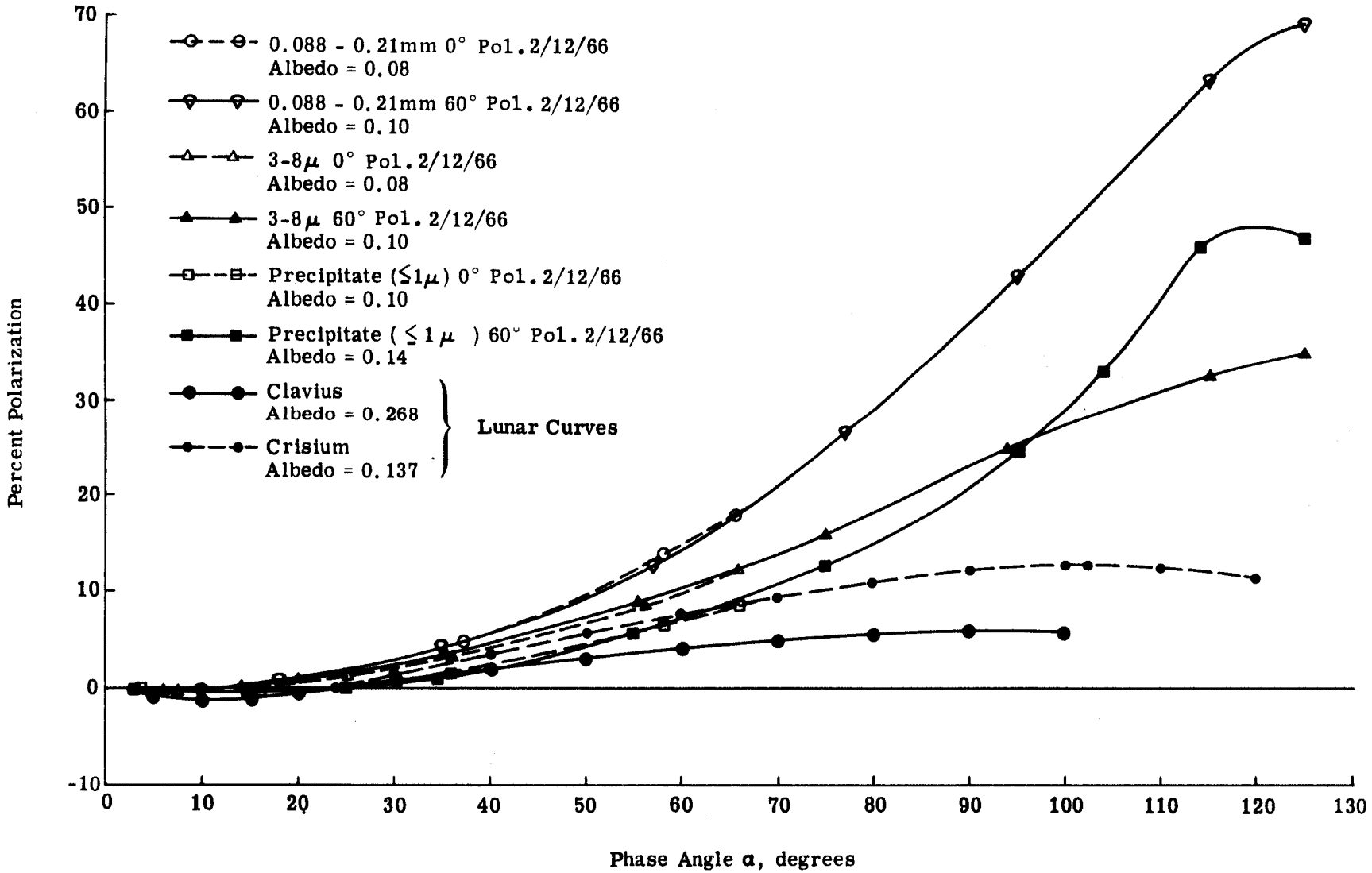

Fig. 20 Silver Chloride (Exposed to Light for Darkening): Percent Polarization as a Function of Particle Size (Uncorrected for Instrumental Effects) 0° and 60° Polarimeters

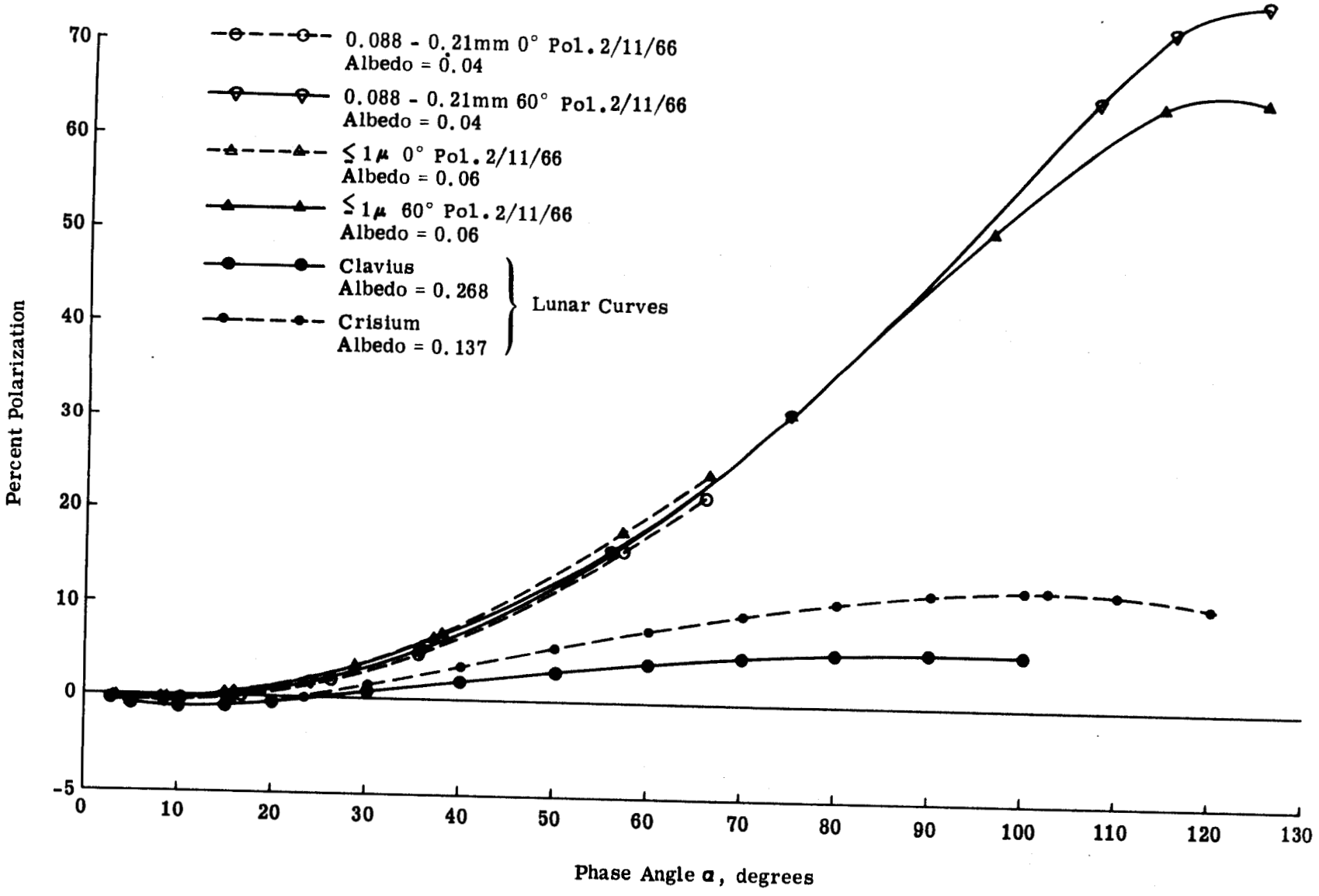

Fig. 21 Copper Oxide: Percent Polarization as a Function of Particle Size (Uncorrected for Instrumental Effects) 0° and 60° Polarimeters

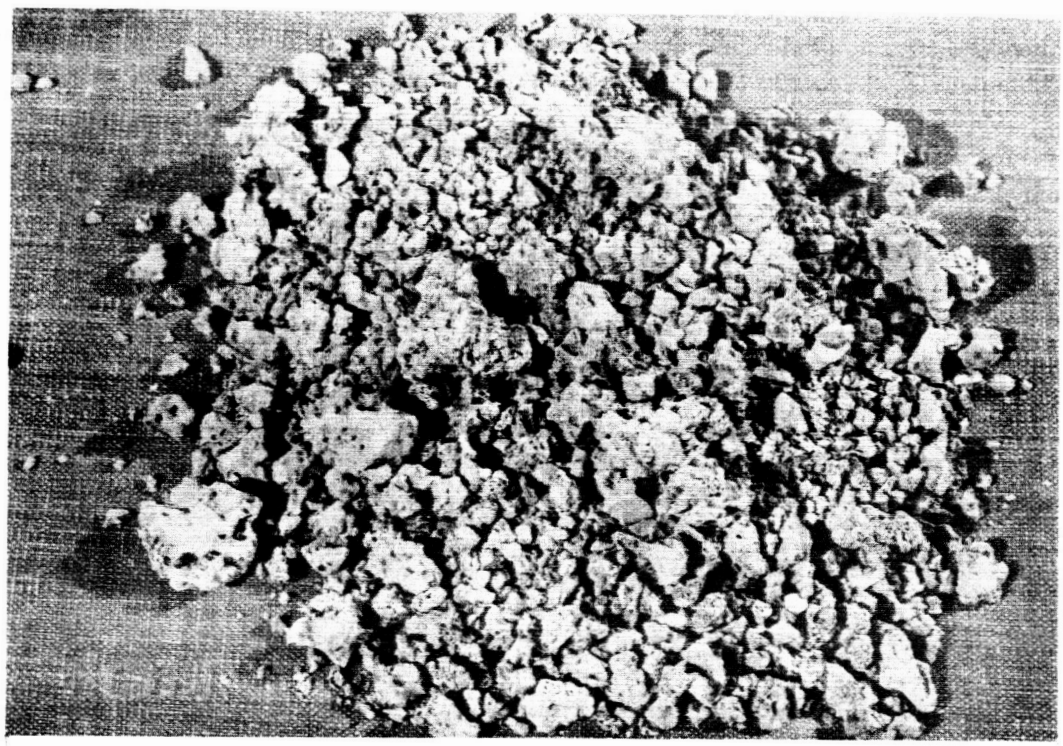

Fig. 22 Volcanic Ash No. 1 (Unpulverized)

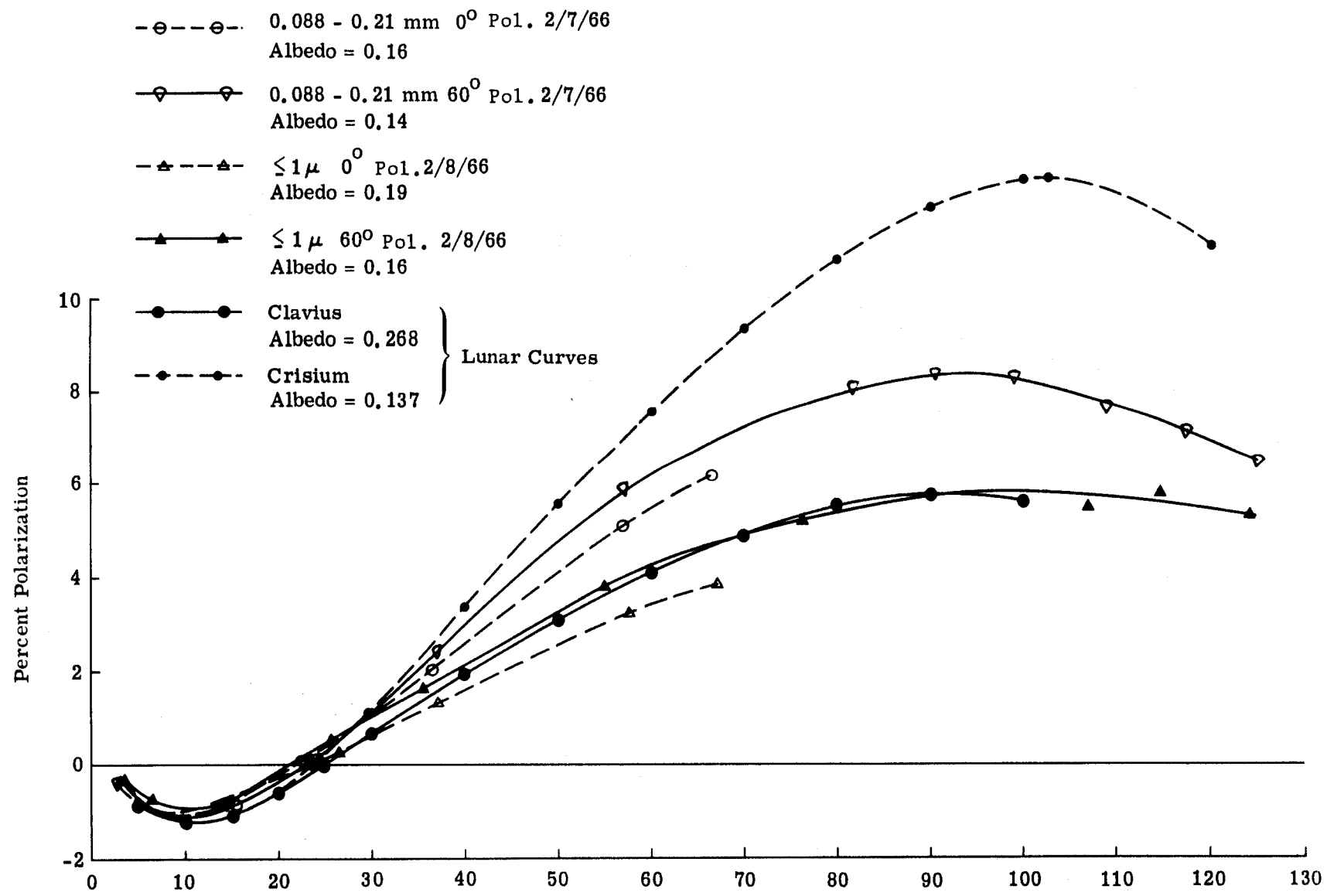

Fig. 23 Volcanic Ash No. 1: Percent Polarization as a Function of Particle Size (Uncorrected for Instrumental Effects) 0° and 60° Polarimeters

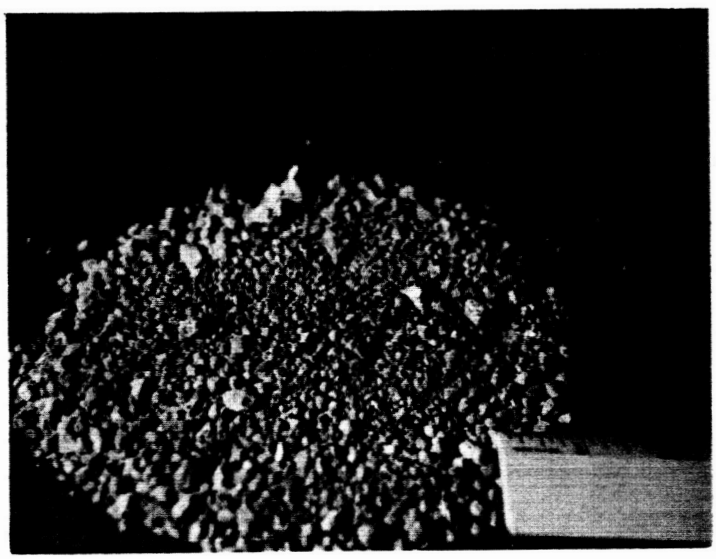

Fig. 24 Vesuvius Cinders (6/1/65)

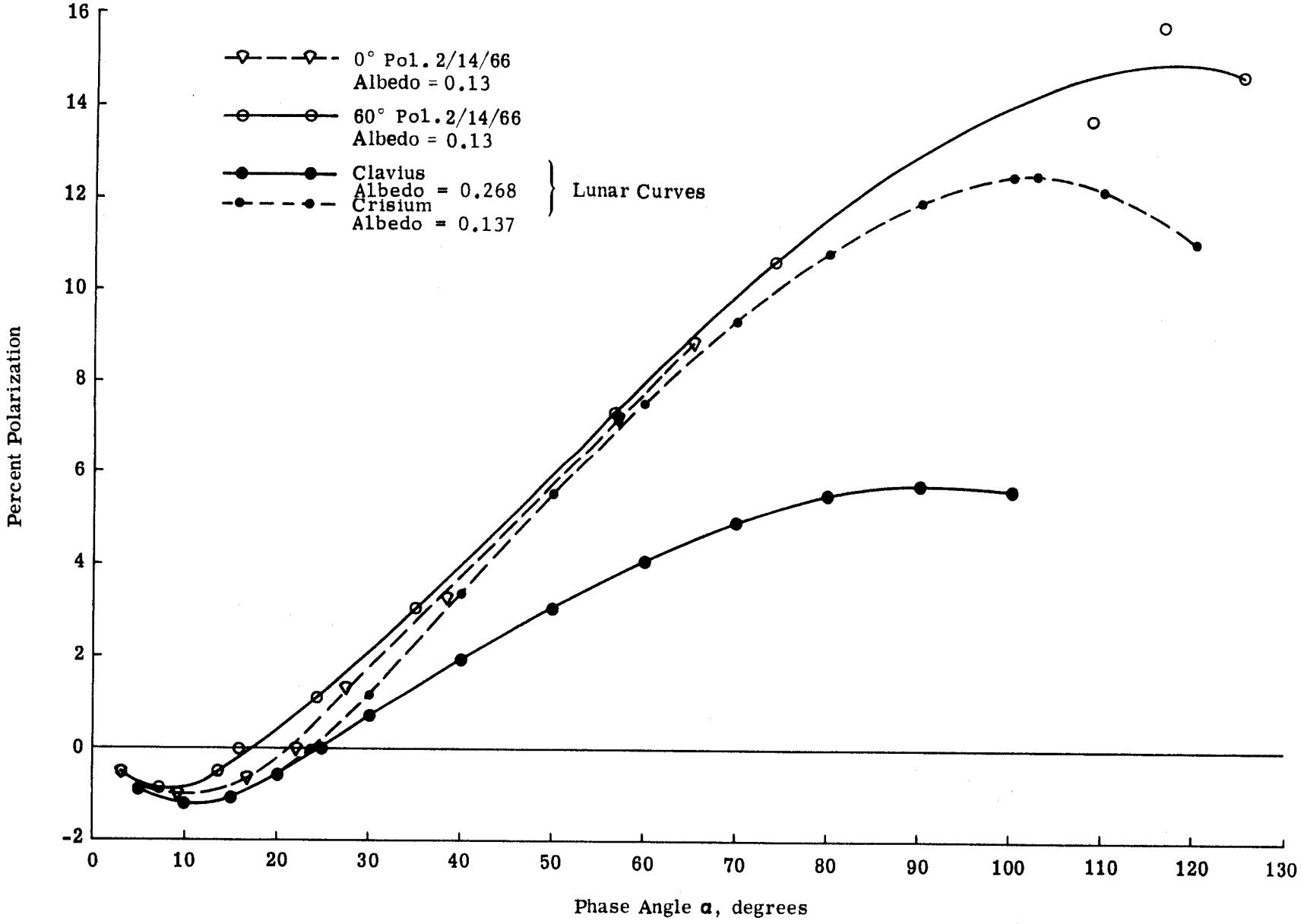

Fig. 25 Vesuvius Cinders (6/1/65): Percent Polarization - 60° Polarimeter

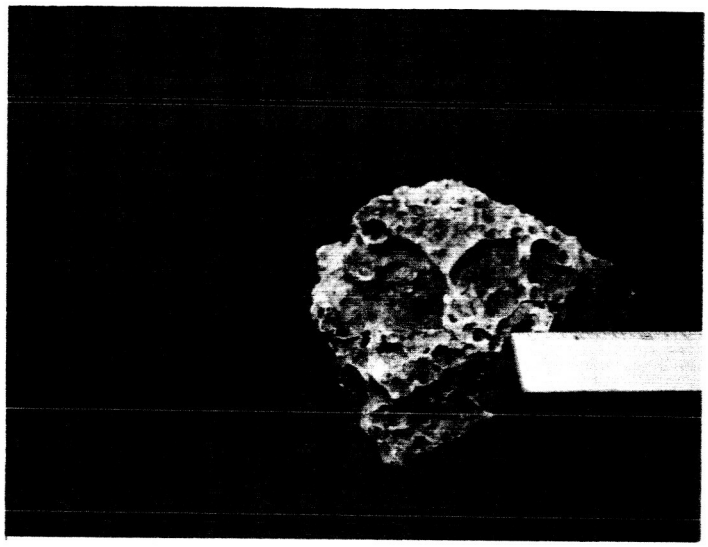

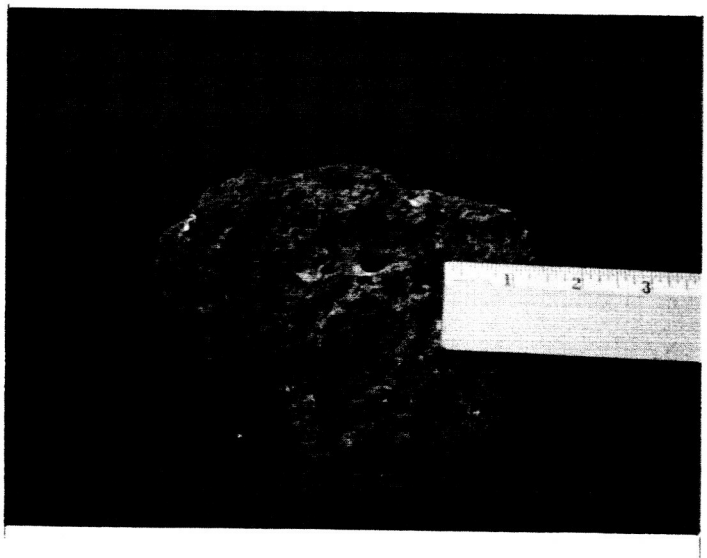

Fig. 26 Furnace Slags (Obtained at NASA/MSC 3/16/65)
Upper - Sponge-like; Lower - Rusty

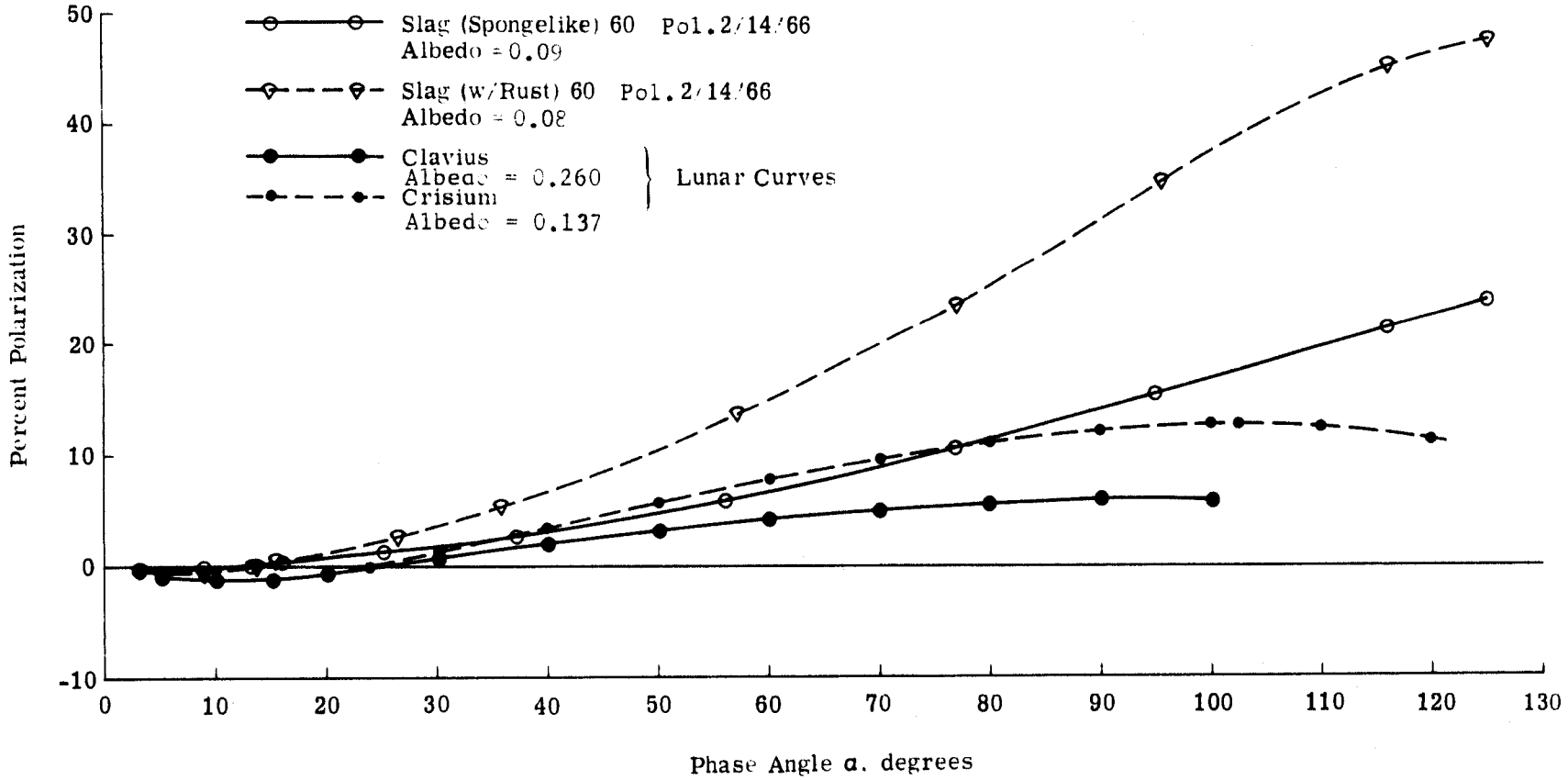

Fig. 27 Furnace Slags (Obtained at NASA/MSC 3/16/65): Percent Polarization - 60° Polarimeter

a) and b) Ashes of Vesuvius April 14, 1908
Lyot Configuration - Thesis p. 120
Curve E; Albedo = 0.166
(Sample Courtesy A. Dollfus)
25μ/div (2-10-66) 63μ/div (2-10-66)

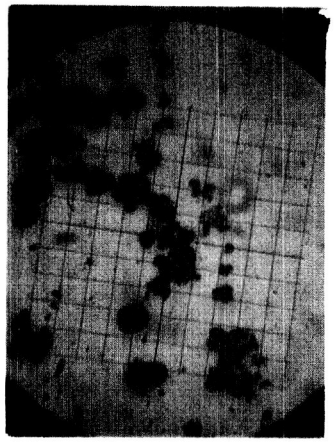

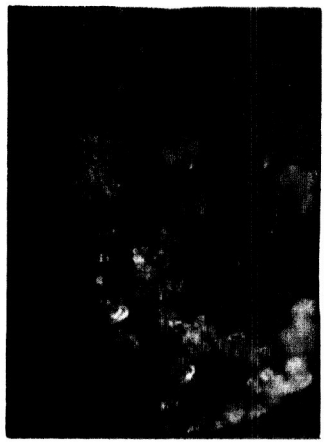

c) and d) Copper Oxide (Various Sizes)
25μ/div (2-10-66) 25μ/div (2-10-66)
(Bright Field Illumination)

e) Coral #1
25μ/div $\leq$ 88μ (2-10-66)

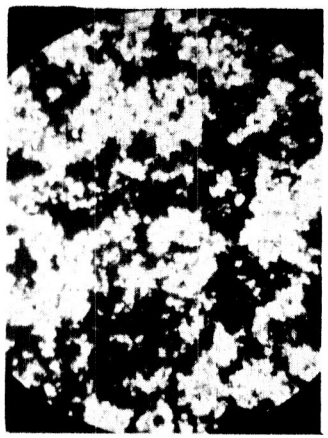

f) Volcanic Ash #1
25μ/div < 88μ (2-10-66)

Fig. 28 Microscopic Photographs of Miscellaneous Specimens - Lyot Volcanic Ash, Copper Oxide, Coral

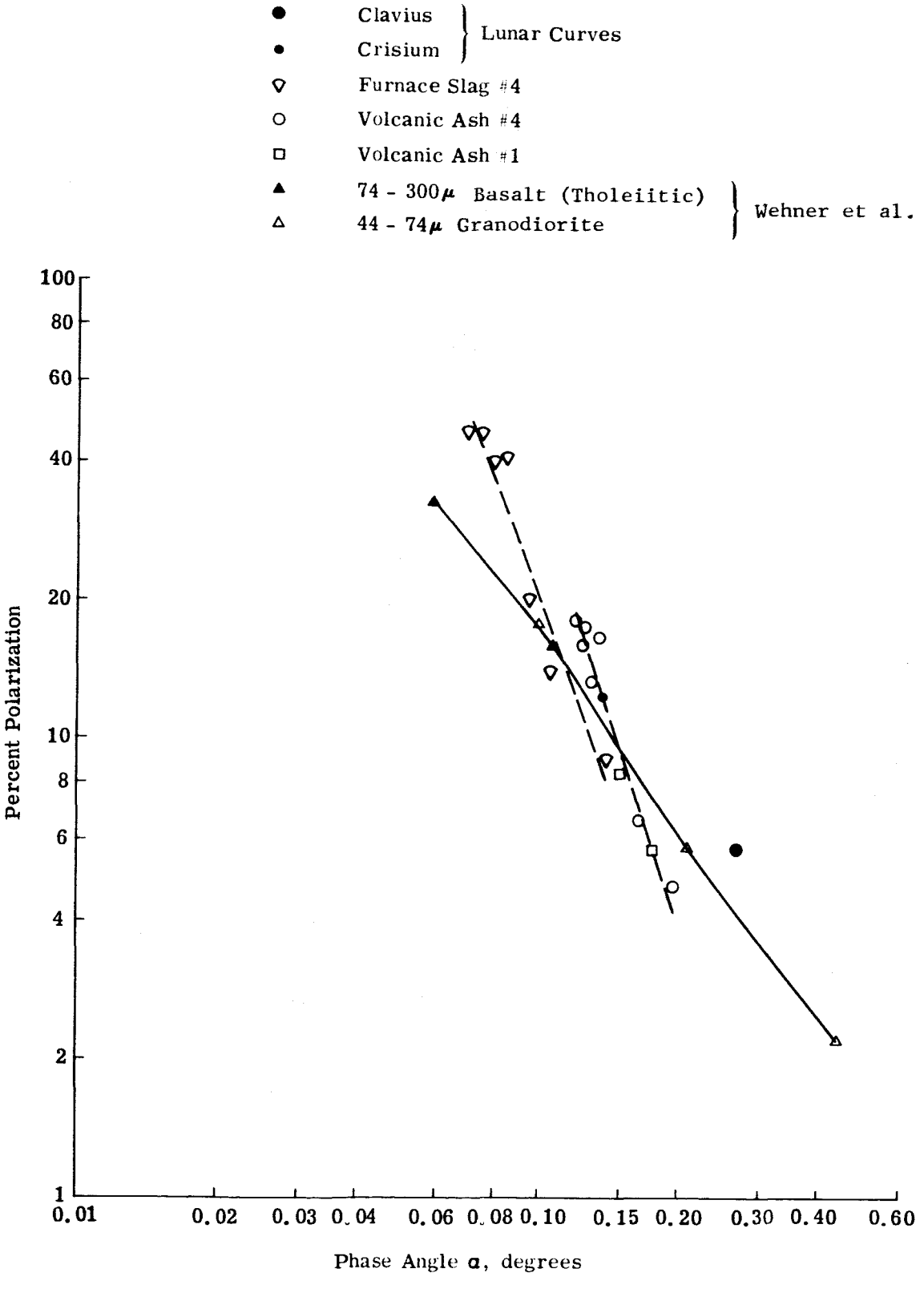

Fig. 29 Maximum Polarizations and Albedos of Various Samples and Lunar Features